CEFLES2: The remote sensing component to quantify photosynthetic efficiency from the leaf to the region by measuring sun-induced fluorescence in the oxygen absorption bands

U. Rascher[1, *], G. Agati[2], L. Alonso[3], G. Cecchi[2], S. Champagne[4], R. Colombo[5], A. Damm[6], F. Daumard[4], E. de Miguel[7], G. Fernandez[3], B. Franch[7], J. Franke[8], C. Gerbig[9], B. Gioli[10], J.A. Gómez[7], Y. Goulas[4], L. Guanter[11], Ó. Gutiérrez-de-la-Cámara[7], K. Hamdi[1], P. Hostert[6], M. Jiménez[7], M. Kosvancova[12], D. Lognoli[2], M. Meroni[5], F. Miglietta[10], A. Moersch[1], J. Moreno[3], I. Moya[4], B. Neininger[13], A. Okujeni[6], A. Ounis[4], L. Palombi[2], V. Raimondi[2], A. Schickling[14], J.A. Sobrino[7], M. Stellmes[15], G. Toci[2], P. Toscano[10], T. Udelhoven[16], S. van der Linden[6], A. Zaldei[10]

[1] Institute of Chemistry and Dynamics of the Geosphere, ICG-III: Phytosphere, Forschungszentrum Jülich, Stetternicher Forst, 52425 Jülich, Germany

[2] IFAC-CNR, Istituto di Fisica Applicata "Nello Carrara", Consiglio Nazionale delle Ricerche, via Madonna del Piano10, I-50019, Sesto F.no, Firenze, Italy

[3] Department of Earth Physics and Thermodynamics, University of Valencia, Dr Moliner, 50, 46100 Burjassot - Valencia, Spain

[4] Laboratoire de Météorologie Dynamique, CNRS, Ecole Polytechnique, 91128 Palaiseau, France

 [5] Remote Sensing of Environmental Dynamics Lab., DISAT, University of Milan-Bicocca, Piazza della Scienza 1, 20126 Milano, Italy

[6] Geomatics Lab, Humboldt-Universität zu Berlin, Unter den Linden 6, 10099 Berlin, Germany

[7] Remote Sensing Laboratory. Instituto Nacional de Técnica Aeroespacial. Carr. de Ajalvir, km 4, 28850 Torrejón de Ardoz, Madrid, Spain.

29   [8] Center for Remote Sensing of Land Surfaces (ZFL), University of Bonn, Walter-Flex-

30   Strasse 3, 53113 Bonn, Germany

31   [9] Max Planck Institute for Biogeochemistry, Hans Knoell Str. 10, 07745 Jena, Germany

32   [10] IBIMET-CNR, Instituto di Biometeorologia, Consiglia Nazionale delle Ricerche, Via G.

33   Caproni 8, 50145 Firenze, Italy

34   [11] Helmholtz Centre Potsdam, GFZ German Research Centre for Geosciences, Department

35   1 - Geodesy and Remote Sensing, Telegrafenberg, 14473 Potsdam, Germany

36   [12] Laboratory of Plants Ecological Physiology, Division of Ecosystem Processes, Institute

37   of Systems Biology and Ecology, Poříčí 3b, CZ-60300 Brno, Czech Republic

38   [13] Metair AG, Flugpaltzm, CH-8915 Hausen am Albis, Switzerland

39   [14] Institute for Geophysics and Meteorology, University of Cologne, Kerpener Str. 13

40   50937 Cologne, Germany

41   [15] Remote Sensing Department, University of Trier, 54286 Trier, Germany

42   [16] CRP-Gabriel Lippmann, Département 'Environnement et Agro-biotechnologies',

43   Geomatic Platform, 41, rue du Brill, L-4422 Belvaux, Luxembourg

44

45   Correspondence to: U. Rascher, e-mail u.rascher@fz-juelich.de, tel. +49-(0)2461-61 2638;

46   fax. +49-(0)2461-61 2492

47

48   **Abstract**

49   The CEFLES2 campaign during the Carbo Europe Regional Experiment Strategy was

50   designed to provide simultaneous airborne measurements of solar induced fluorescence and

51   CO_2 fluxes. It was combined with extensive ground-based quantification of leaf- and canopy-

52   level processes in support of ESA's Candidate Earth Explorer Mission of the 'Fluorescence

53   Explorer' (FLEX). The aim of this campaign was to test if fluorescence signal detected from

54   an airborne platform can be used to improve estimates of plant mediated exchange on the

55   mesoscale. Canopy fluorescence was quantified from four airborne platforms using a

56   combination of novel sensors: (i) the prototype airborne sensor AirFLEX quantified

57   fluorescence in the oxygen A and B bands, (ii) a hyperspectral spectrometer (ASD) measured

58   reflectance along transects during 12 day courses, (iii) spatially high resolution georeferenced

59   hyperspectral data cubes containing the whole optical spectrum and the thermal region were

60   gathered with an AHS sensor, and (iv) the first employment of the high performance imaging

61   spectrometer HYPER delivered spatially explicit and multi-temporal transects across the

62   whole region. During three measurement periods in April, June and September 2007

63   structural, functional and radiometric characteristics of more than 20 different vegetation

64   types in the Les Landes region, Southwest France, were extensively characterized on the

65   ground. The campaign concept focussed especially on quantifying plant mediated exchange

66   processes (photosynthetic electron transport, CO_2 uptake, evapotranspiration) and

67   fluorescence emission. The comparison between passive sun-induced fluorescence and active

68   laser-induced fluorescence was performed on a corn canopy in the daily cycle and under

69   desiccation stress. Both techniques show good agreement in detecting stress induced

70   fluorescence change at the 760 nm band. On the large scale, airborne and ground-level

71   measurements of fluorescence were compared on several vegetation types supporting the

72   scaling of this novel remote sensing signal. The multi-scale design of the four airborne

73   radiometric measurements along with extensive ground activities fosters a nested approach to

74   quantify photosynthetic efficiency and gross primary productivity (GPP) from passive

75   fluorescence.

76

1 Introduction

Photosynthesis harvests light from a variable stream of solar photons and converts this energy to carbohydrates that fuel all plant processes and ultimately life on Earth. The efficiency of photosynthetic electron transport and carbon fixation is highly regulated, depending on plant species and environmental constrains (Rascher & Nedbal, 2006; Schurr et al., 2006). Quantum efficiency of photosystem II (PSII) depends primarily on light intensity and varies between 0.83 at leaves of dark adapted higher plants to close to zero at high light intensities (Rascher et al. 2000). Plants have evolved a variety of photochemical and non-photochemical regulation mechanisms that are either constitutively active or are activated on demand to optimise the distribution of energy for photosynthesis and to avoid damage because of over-energetisation of metabolism (Schulze & Caldwell, 1995 for a comprehensive summary). Thus, plant photosynthesis is dynamically regulated adapting to environmental conditions and being affected by the ecological plasticity of each species (Turner et al., 2003b; Schurr et al., 2006).

Remote sensing offers the unique possibility to derive spatially explicit information on vegetation status at local, regional or landscape scale (Goetz and Prince, 1999; Hilker et al., 2008). Reflectance signals alone, however, cannot quantify photosynthetic activity and dynamics of vegetation accurately. Great benefits would be expected from remote sensing techniques that quantify the actual status of photosynthetic carbon fixation. Monteith´s (1972; 1977) mechanistic Light Use Efficiency (LUE) concept relates the photosynthetic capacity to LUE, describing the potential to convert absorbed radiation into biomass. Accordingly, gross primary productivity (GPP) can be described as a function of the fraction of absorbed photosynthetic active radiation (f_{APAR}) and LUE (Turner et al., 2003a; Hilker et al., 2008). LUE is highly variable and depends on the phenological status, structure and species composition (Field et al., 1995; Goetz and Prince, 1999). Due to its dynamic changes, the insufficient parameterization of LUE is identified as a major source of uncertainties in modeling GPP (Hilker et al. 2008, Running et al., 2000).

Chlorophyll fluorescence analyses are among the most powerful techniques to non-destructively quantify photosynthetic efficiency and non-photochemical energy dissipation in photosynthetically active organisms under laboratory conditions. At canopy and field scale, chlorophyll fluorescence emission is frequently considered to be employed as a complementary, high-capacity signal on vegetation dynamics (Papageorgiou and Govindjee,

2004). Sun-induced fluorescence can be obtained from remote sensing platforms. Several studies have shown that it is correlated with photosynthetic efficiency and thus may serve as a proxy to quantify photosynthetic efficiency (Flexas et al., 2000, 2002).

The chlorophyll fluorescence emitted by a leaf under natural sunlight is only 1-5 % of the total reflected light at a specific wavelength. This makes it particularly difficult to quantitatively extract the fluorescence signal from remote sensing data. However, at certain wavelengths, the solar irradiance is absorbed in the solar or earth atmosphere (so-called Fraunhofer lines); thus, there is no or greatly reduced incoming radiation at the Earth's surface in these wavelengths (Plascyk, 1975). Solar irradiance exhibits three main absorption bands in the red and near infrared wavelength region: the Hα line at 656.3 nm is due to hydrogen absorption in the solar atmosphere, whereas two bands at 687 (O_2-B) and 760 nm (O_2-A) are due to absorption by molecular oxygen in the terrestrial atmosphere. The O_2-A and O_2-B bands especially overlap with the chlorophyll fluorescence emission spectrum and, due to their widths, have the potential to be investigated from air- and space-borne platforms. Thus, they can be used for monitoring chlorophyll fluorescence emission under daylight excitation by the method of the Fraunhofer lines in-filling (Plascyck, 1975).

Several studies are currently under way to evaluate the accuracy with which sun-induced fluorescence can be used to quantify photosynthetic efficiency. With this paper we report the concept and first results from the CEFLES2 campaign that took place in the context of the Carbo Europe Regional Experiment between April and September 2007 in Southern France (see http://www.esa.int/esaLP/SEMQACHYX3F_index_0.html). This campaign combined state-of-the-art remote sensing with extensive field-based measurements to quantify the actual status of photosynthetic efficiency from the level of single leaves to a regional scale. The overarching goal was to better constrain and reduce uncertainties in modelling mesoscale carbon fluxes using fluorescence as a direct input parameter.

2   The integrated concept of CEFLES2: quantifying photosynthetic efficiency from leaf- to the regional scale

CEFLES2 was designed to provide extensive and spatially resolved validation of photosynthesis estimates based on remote sensing fluorescence measurements that can be obtained using airborne instrumentation. Validation data were provided by extensive ground

140 measurements of plant mediated exchange processes (photosynthetic CO_2 uptake,
141 evapotranspiration and water use efficiency), fluorescence features at the leaf and canopy
142 scale, and by CarboEurope aircraft fleet that was operating during CERES experimental
143 campaigns in Les Landes (France) in April and September 2007.

144 A multitude of vegetation specific ground measurements were acquired during three
145 campaigns (April, June, and September 2007). These included structural parameters (leaf area
146 index (LAI), canopy height or fractional cover (f_{cover}), biochemical characterizations
147 (chlorophyll, water and dry matter content), physiological parameters (PAM fluorometry, gas
148 exchange) and standard field spectroscopy. These more traditional measurements were
149 complemented with novel set-ups aimed to quantify fluorescence at the canopy level. As
150 species of major interest, winter wheat was chosen in April and corn in September.
151 Additionally, investigations were expanded to rapeseed, grassland and pine in April, corn,
152 potato, sunflower and pine in June and bean, kiwi, vine and oak forest in September. The
153 intensive measurement site was Marmande during the whole CEFLES campaign. Further test
154 sites were located in Clairac, Le Bray, Villeneuve-sur-Lot, and Saint Laurent du Bois.

155

2.1 Leaf-level: Quantifying photosynthesis and fluorescence

2.1.1 PAM fluorometry to derive cardinal points of photosynthesis

158 Efficiency of light reactions of photosynthesis were measured on the level of single leaves
159 using the miniaturized Fluorescence Yield Analyser (Mini-PAM) of H. Walz (Effeltrich,
160 Germany) with a leaf clip holder described by Bilger, Schreiber and Bock (1995) (Fig. 1A).
161 Spot measurements of photosynthetic photon flux density (PPFD, $\lambda = 380$ nm to 710 nm)
162 were taken inside the measuring field by the micro-quantum sensor of the Mini-PAM.
163 Effective quantum yield of PS II ($\Delta F/F_m'$) was calculated as (F_m' - F) / F_m', where F is
164 fluorescence yield of the light adapted sample and F_m' is the maximum light-adapted
165 fluorescence yield when a saturating light pulse (800 ms duration, intensity ≈ 4000 µmol m^{-2}
166 s^{-1}) was superimposed on the prevailing environmental light levels. The apparent rate of
167 photosynthetic electron transport (ETR) of photosystem II (PS II) was obtained as
168 ETR = $\Delta F/F_m' \cdot PPFD \cdot 0.5 \cdot \alpha$, where the factor 0.5 assumes equal excitation of both

169 photosystems; the absorption factor α was derived from leaf level optical measurements using

170 an integrating sphere.

171 Light within the canopy constantly changed and showed patches of varying intensity. Thus,

172 leaves were exposed to rapid changes in PPFD of various duration and intensity, which could

173 not be determined analytically. $\Delta F/F_m'$ and ETR values dynamically adapt primarily to these

174 changes in light intensity, but may also reflect manifold underlying physiological

175 mechanisms. Additional parameters, such as maximum apparent electron transport rate

176 (ETR_{max}) and saturating photosynthetically active radiation can be derived from light-

177 response curves. In general, measurements of light-response curves lead to a deeper insight

178 into characteristic parameters of a plant species, which are not related to the momentary

179 ambient light conditions, but rather to the ontogeny of a leaf and to the range of physiological

180 plasticity of a plant. In order to obtain light response characteristics, about 100 randomly

181 distributed spot measurements were recorded within a field and plotted over PPFD. Light

182 dependency data plotted in such way were mathematically fitted using single exponential

183 functions to quantify the characteristic cardinal points of photosynthesis (Rascher et al. 2000).

184

185 ## 2.1.2 Measurement of fluorescence emission spectrum

186 Algorithms for fluorescence retrieval from airborne data require the characterization of the

187 fluorescence emission spectrum at the leaf level. They were recorded under natural sun light

188 conditions using a specially built spectro-fluorometer based on a HR2000+ spectro-

189 radiometer (Ocean Optics). (Fig 1H). This instrument used solar radiation as an excitation

190 source. Solar radiation is filtered by a short pass blue filter and focused onto the leaf by a

191 converging lens to compensate the attenuation of the filter.

192 The spectro-radiometer was calibrated spectrally and for linearity using a standard black body

193 (LI-Cor 1800-02, NE, USA) and a Hg-Ar standard lamp (CAL-2000, Micropack, Germany).

194 Measurements were performed around solar noon and during overflights in April, June and

195 September 2007 on grass, wheat, corn and bean leaves from the different experimental sites.

196 Chlorophyll content and PPFD were systematically acquired with a chlorophyll-meter

197 (SPAD-502, Minolta) and a quantum-meter.

198

2.2 Canopy-level

2.2.1 Active laser induced fluorescence

Active fluorescence spectra of vegetation were recorded by using a hyperspectral Fluorescence LIDAR (FLIDAR) imaging system (Fig. 1C). This consists mainly of a Q-switched Nd:YAG laser, a 1 m focal length Newtonian telescope and a 300 mm focal length spectrometer coupled to an intensified, gated 512×512 pixels CCD detector. Imaging was carried out by scanning the target with a computer-controlled motorized mirror. The FLIDAR prototype includes also a low power DPSS (Diode-Pumped Solid State) laser (emitting in the green) for geometrical referencing on the target.

The pulsed Nd YAG laser excitation source can operate at 355 nm (triple frequency) or at 532 nm (double frequency), with pulse width of 5 ns, pulse energy of 8 mJ and 20 mJ for the UV and green excitation respectively, and maximum repetition rate of 10 Hz. The laser beam divergence is 0.5 mrad with a starting beam diameter of 7 mm. Three folding high energy dielectric mirrors provide the excitation laser beam to be coaxial to the telescope. The telescope is a 25 cm diameter f/4 Newtonian reflector. The fibre bundle is composed by 50 quartz optical fibres with a core diameter of 100 μm. The far field of view is 1 mrad that corresponds to about 2 cm diameter circle spot at a distance of 20 m.

The spectral dispersion system is the flat field SpectraPro-2300i by Acton Research. This spectrometer has a crossed Czerny Turner layout, 300 mm focal length, f/4. The spectrometer is equipped with three dispersion gratings having 150, 600, and 2400 grooves mm^{-1}. The gratings provide a nominal dispersion of 21.2, 5.1 and 0.9 nm mm^{-1}, respectively. The detector is a gateable 512x512 pixel CCD (model PI MAX:512, Princeton Instruments/Acton) equipped with an intensifier (Unigen III Generation). The pointing and scan system for the hyperspectral imaging is obtained by a movable folding mirror placed between the telescope and the target. This mirror is mounted in a controllable motorized fork that permits the rotation on two orthogonal axes. The primary axis is fixed and coaxial with the telescope and crosses the geometrical centre of the folding mirror surface. The secondary axis direction is set by the rotation of the first one, coplanar with mirror surface and crossing its geometrical centre. The used stepping motors give rotation accuracy better than 0.5 mrad.

229 Two different field set-ups of the FLIDAR were used to take measurements on vegetation: the
230 first one, adopted during the April campaign, relied on the use of 4 mirrors positioned at 45°
231 at about 1 m above the canopy (Fig. 1B). Wheat fluorescence was excited at 355 nm and
232 detected in the 570 – 830 nm and 348 – 610 nm spectral windows. The 4 canopy zones (560
233 cm^2 each) were covered by scanning the motorized mirror, placed near the optical sensor that
234 was mounted inside a van. A 10x10 sampling grid (~100 points per zone) was adopted and a
235 spectrum was obtained by averaging 30 spectra per point.

236 The second one, adopted during the September CEFLES2 campaign, used a scanning mirror
237 positioned on the top of a 6-m high scaffolding tower (Fig. 1D). This configuration, with the
238 mobile mirror at about 2.7 m above the canopy, permitted to cover 1 m^2 area of the corn field
239 within small angles from nadir. A reference fluorescent plastic target (Walz, Effeltrich,
240 Germany, about 10x10 cm^2 of size) was positioned on the top-left corner of the scanned area;
241 its fluorescence signal was acquired once per each area scan, and used to normalize the
242 fluorescence spectra of the scanned area. The van with the laser was located at about 10 m
243 from the scaffolding tower.

244 In both set-ups, the canopy average temperature was continuously measured and logged by
245 means of a Minolta Land Cyclops optical pyrometer mounted either in proximity of the four
246 45° mirrors (Fig. 1B) or on top of the scaffolding tower (Fig. 1D).

247

248 < Figure 1 >

249

250 2.2.2 Passive sun-induced fluorescence

251 Sun-induced fluorescence (Fs) was estimated in the field with four different set-ups. Three
252 stationary set-ups exploit field spectrometers to collect the signal above the canopy during the
253 day and differ for the spectral resolution achieved. While the first one was manually operated,
254 the second and third system operated autonomously. In addition to the stationary approaches,
255 a mobile set-up was used to quickly measure the distribution of canopy fluorescence and thus
256 cover the spatial distribution of the F_S signal.

257 (1) The core of the first set-up was composed by two HR4000 spectrometers (OceanOptics,
258 USA). One spectrometer covered the visible to near-infrared part of the spectrum (350 -

259   1100 nm) with a resolution of 2.8 nm (Full Width at Half Maximum, FWHM) while a second

260   spectrometer was limited to a narrower spectral range in the near-infrared (720 – 800 nm) to

261   provide a very high spectral resolution (0.13 nm FWHM) intended for fluorescence retrieval

262   at the O_2-A band. The canopy was observed from nadir by bare fibres (25° field of view). The

263   manual rotation of a mast mounted horizontally on a tripod permitted to observe either the

264   white reference panel or the canopy. The spectrometric set-up was installed over winter

265   wheat in April and over corn in September to record canopy diurnal cycle of optical

266   properties and sun-induced fluorescence. (Fig. 1F refers to the set-up used in the September

267   over corn).

268   Prior to the field campaign both spectrometers were calibrated with known standards

269   wavelength calibration and radiance calibration. The spectroscopy technique referred to as

270   'single beam' (Milton and Rolling, 2006) was applied in the field to evaluate the incident and

271   upwelling fluxes: target measurements are 'sandwiched' between two white reference

272   measurements (calibrated panel, Optopolymer GmbH, Germany) taken a few seconds apart.

273   For every acquisition, 15 and 4 scans (for the two spectrometers, respectively) were averaged

274   and stored as a single file. Additionally, a dark current measurement was collected for every

275   set of acquisitions (four consecutive measurements). Spectrometers were housed in a Peltier

276   thermally insulated box (model NT-16, Magapor, Zaragoza, Spain) keeping the internal

277   temperature at 25°C in order to reduce dark current drift.

278   Processing of raw data included correction for CCD detector non linearity, correction for dark

279   current drift, wavelength calibration and linear resampling; radiance calibration, incident

280   radiance computation by linear interpolation of two white reference panel measurements, and

281   computation of vegetation optical indices and sun-induced fluorescence according to Meroni

282   and Colombo (2006).

283

284   (2) A second high performance spectro-radiometer set-up (SpectroFLEX) for detecting

285   passive fluorescence signal has been installed at Villeneuve-sur-Lot (Lat. 44.397571°, Long.:

286   0.763944°) during April 2007, in the middle of a large and homogeneous field of natural grass

287   (Fig. 1E). The objective was to compare passive fluorescence data acquired with the airborne

288   AirFLEX sensor with similar data acquired on ground on the same target. The target was

289   composed mainly of Velvetgrass (*Holcus lanatus)*, an erectophil monocot species of about 60

290   cm height.

291   SpectroFLEX is based on a narrow band spectrometer (HR2000+, Ocean Optics, USA). The

292   instrumental function of 0.2 nm FWHM was established using the atomic lines of a spectral

293   calibration lamp (Cal-2000-Bulb, Micropack, Germany) also used for wavelength calibration.

294   Radiometric calibration has been performed with a black body lamp (Li-Cor 1800-2, Lincoln,

295   NE, USA). A high pass filter (Schott RG590) prevented for stray light. The spectro-

296   radiometer was enclosed in a temperature regulated box at $25 \pm 0.5\,°C$, allowing thermal

297   noise reproducibility. A shutter (Inline TTL shutter, Micropack, Germany) allows CCD dark

298   current acquisition for each integration time. All the electronic components were protected by

299   a waterproof aluminium box. Fluorescence fluxes were simultaneously acquired in both O_2-B

300   band (687 nm) and O_2-A band (760 nm), similar to the AirFLEX sensor. Fluorescence was

301   computed using the same channel widths and positions as the AirFLEX sensor inboard the

302   Seneca airplane. SpectroFLEX has been designed to measure automatically over extended

303   periods of time (days or weeks).

304   Measurements at the canopy level required a nadir viewing configuration. The instrument box

305   was installed in the top of a 2.5 m scaffolding. A 2 m length optical fibre connects the sensor

306   head to the spectrometer. The entrance of the optical fibre is fixed above the target by a 1 m

307   horizontal arm at 2.4 m above the ground (Fig. 1E). The resulting target diameter is about 1.1

308   m which ensures a good spatial integration of the canopy structure. Local irradiance was

309   measured using a white frosted PVC board which intercepts alternately the field of view of

310   the sensor. This reference board was periodically moved by an electromagnet. Radiances

311   measured with the reference board were used to estimate the photosynthetic active radiation

312   after calibration against a quantum meter (SDEC, France). An elementary measurement cycle

313   requires the acquisition of two spectra on the target and two spectra on the reference. The

314   acquisition frequency is up to 0.4 Hz at maximum illumination.

315

316   (3) A FieldSpec Pro high resolution spectroradiometer (Analytical Spectral Devices, Boulder,

317   USA), which measures reflected radiation within the spectral domain of 350-2500 nm with a

318   nominal bandwidth of 1.4 nm (350-1050 nm) and a field-of-view (FOV) of 25°. A calibrated

319   Spectralon™ panel (25x25 cm) served as white reference to estimate incident irradiance.

320   The instrument's fibre optic was mounted on a robotic arm of 0.6 m length, approximately

321   1 m above the canopy. The movement of the robotic arm allowed to automatically collecting

322   daily cycles of four different spots with a circular area of about 0.5 m diameter each (Fig.

323 1G). The acquired dataset consists of spectral records from four canopy areas, bracketed by

324 measurements of the reference panel. At each position, a trigger signal released the recording

325 of 10 single spectra. Each spectrum was internally averaged by the spectrometer from 25

326 individual measurements. Integration time was automatically optimized during the day in

327 order to maximize the instrument signal to noise ratio. In June and September five diurnal

328 courses were acquired during the campaign windows. The fluorescence signal was quantified

329 using the modified FLD method proposed by Maier et al. (2003) in the O_2-A band.

330

331 (4) Several FieldSpec Pro high resolution spectroradiometers were used for a spatially explicit

332 characterization of the fluorescence signal over a wide range of agricultural crops and surface

333 classes. During the three campaigns in April, June, and September 11 different crops were

334 characterized, whereas one representative field per crop was selected (exceptionally winter

335 wheat with seven fields and corn with eight fields). Beside these agricultural canopies, water

336 and bare soil were measured. To cover the spatial heterogeneity of each field, four

337 representative places were selected and three measurements per place were performed.

338 At each place in the field, the instrument's fibre optic was mounted on a tripod,

339 approximately 1 m above the canopy. Three different spots with a circular area of 0.5 m

340 diameter each were recorded moving the fibre optic manually over the canopy. The

341 fluorescence signal was quantified as mentioned in set-up 3.

342

343 ## 2.2.3 Quantifying sun-induced fluorescence using the Fraunhofer Line

344 Discrimination

345 Under natural sunlight illumination, chlorophyll *a* exhibits a fluorescence emission spectrum

346 in the red and near-infrared regions (600 – 800 nm), characterized by two peaks at about 690

347 and 740 nm. Solar light is reflected by vegetation in the same spectral region (Fig. 2) and

348 therefore the signal reaching a remote sensor is composed by the superimposition of the two

349 fluxes: fluorescence and background reflection from the surface.

350

351   < Figure 2 >

352

353 In laboratory conditions, one can somehow decouple the two signals by selecting two non

354 overlapping wavelengths for illumination and observation of the sample: a shorter excitation

355 wavelength induces fluorescence which is observed at longer wavelength without any

356 reflection background (e.g. Corp et al., 2006). This concept has been also successfully

357 adapted for outdoor application using a pulsed laser as light source for measuring the so-

358 called laser induced fluorescence (see Section 2.2.1). However, this approach cannot be

359 currently considered for satellite observations because it requires a strong laser pulse that

360 limits its application to the near range.

361 Fluorescence quantification from the far range must rely on passive measurements (i.e.

362 without the use of an artificial excitation source) to decouple the small fluorescence signal

363 from the background reflectance. This goal can be achieved by selectively measuring the flux

364 upwelling from vegetation in specific spectral lines characterised by very low levels of

365 incident irradiance (i.e. Fraunhofer lines).

366 In such lines the otherwise much stronger reflectance background is significantly reduced,

367 and fluorescence can be decoupled from the reflected signal. In particular, two of these lines

368 (O_2-B and O_2-A positioned at 687 and 760 nm and due to oxygen absorption in the earth

369 atmosphere) largely overlap with the chlorophyll fluorescence emission spectrum of plants

370 and have often been exploited for fluorescence retrieval (e.g. Moya et al., 1999; Evain et al.

371 2001, Moya et al. 2004, Louis et al., 2005; Meroni et al., 2008; Middleton et al., 2008).

372 Fluorescence is estimated in correspondence of these spectral lines by using the FLD

373 (Fraunhofer Line Discrimination) method originally proposed by Plascyck (1975). In short,

374 this method compares the depth of the line in the solar irradiance spectrum to that of the line

375 in the radiance spectrum up-welling from vegetation. Fluorescence is quantified by measuring

376 to what extent this depth is reduced by fluorescence in-filling. In operation, fluorescence can

377 be decoupled from the reflected signal when measuring in spectral channels close enough so

378 that it can be assumed that both reflectance and fluorescence vary smoothly with wavelength.

379 Therefore, FLD relies on spectral measurements inside and outside narrow Fraunhofer lines,

380 in which incident irradiance is strongly reduced.

381 The FLD basic concept has been recently upgraded with several modifications and

382 improvements by different research groups (e.g. Gomez-Chova et al., 2006; Meroni and

383 Colombo, 2006; Alonso et al., 2008) in order to increase the accuracy of the method and to

384   exploit the current availability of hyperspectral high resolution data (for a review of

385   fluorescence retrieval method see Meroni et al., submitted).

386

387

388   2.3   Field to regional level using novel airborne sensors

389   On the largest spatial scale, a fleet of several aircrafts was employed over the region testing

390   different approaches to quantify sun-induced fluorescence from airborne platforms (Fig. 3).

391

392   < Figure 3 >

393

394   2.3.1 Repeated transects using AirFLEX

395   AirFLEX is an interference-filter based airborne sensor developed in the framework of the

396   Earth Observation Preparatory Programme of the European Space Agency (Fig 3A-C).

397   Basically it is a six channel photometer aimed to measure the in-filling of the atmospheric O_2

398   bands. A set of 3 different channels (each with a specific interference filter) is used to

399   characterize each absorption band: one at the absorption peak and two others immediately

400   before and after the O_2 absorption feature. The peak positions of these filters (Omega Optical,

401   Brattleboro, VT, USA) are 685.541, 687.137 and 694.114 nm for the O_2-B band and 757.191,

402   760.39 and 770.142 nm for the O_2-A band (L1 to L6, respectively, Fig. 2 bottom). The

403   FWHM are 0.5 nm and 1.0 nm for the O_2-B and O_2-A band respectively. In order to maintain

404   stability of the characteristics of these filters, the filter compartment was insulated and

405   warmed up to 40°C +/-0.1°C. The use of two filters out of the band allows interpolating the

406   reflectance within the band. In addition to the narrow band filters, long pass coloured filters

407   (Schott RG645) in combination with a baffled hub are used to reduce the stray light.

408   The AirFLEX sensor was fixed on the floor of the Piper Seneca airplane of the IBIMET (Fig.

409   3B). During data acquisition a synchronised video camera recorded the images of the context

410   and a spectroradiometer measured the radiance of the target in the spectral range of 200 – 890

411   nm. A proprietary program developed under LABVIEW 7 (National Instrument) software

412   allows for real time control and display of measured signals. AirFLEX has been calibrated

413 radiometrically, with a calibration source (Li-Cor 1800-02, NE, USA). The spectral
414 calibration was done with an HR4000 spectrometer (Ocean Optics, IDIL, France) and 6035
415 Hg(Ar) lamp (Oriel Instruments, France). The foot print on the ground is about 10x15m at a
416 repetition rate of 5 Hz. The entire CEFLES2 campaign totalised 14 flights performed by the
417 Seneca aircraft with the AirFLEX sensor onboard, which represent a ground sampling of
418 about 6000 km. AirFLEX generated several products including (i) fluorescence radiances at
419 687 and 760 nm, (ii) fluorescence fractions at the same wavelengths obtained by dividing
420 fluorescence radiances by the reflected radiance at 687 nm, (iii) the Photochemical
421 Reflectance Index (PRI, Gamon et al., 1992) and (iv) the Normalized Differential Reflectance
422 Index (NDVI). A commercial thermal camera (Flir, mod. SC500) was installed together with
423 AirFLEX providing surface temperature information coregistered with fluorescence data (Fig.
424 3C).

425

2.3.2 Repeated transects using an airborne hyperspectral sensor in the METAIR-DIMO aircraft.

428 The small research aircraft of Metair AG (Switzerland) was used as platform for hyperspectral
429 measurements. Alongside an extensive range of additional parameters such as CO_2, H_2O, CO,
430 NOx, (Neininger, 2001, Schmitgen et al., 2004) were captured simultaneously. The flight
431 track and attitude angles were recorded by a TANS Vector phase sensitive GPS system
432 blended with 3-axis accelerometers. For the collection of hyperspectral reflectance data, a
433 portable sensor (FieldSpec Pro, ASD Inc., Boulder, CO, USA) was mounted in the lefthand
434 underwing pod (Fig. 3G). Reflected light was captured in nadir orientation with a fibre optic
435 that was equipped with a 1° foreoptic. Incident light was spectrally analyzed in the range from
436 350 to 1050 nm, with a FWHM of 1.4 nm. The instrument was operated in continuous mode,
437 thus spectra were collected with approximately 2 Hz. Spectral measurements were recorded
438 using radiances and exposure time was adjusted to 130 ms for best signal to noise ratio and to
439 avoid saturation. In order to improve data quality, three spectra were averaged and saved. The
440 FieldSpec device generates a TTL trigger signal that was used (i) to record the time of each
441 hyperspectral measurement and (ii) to capture a video image (640 x 480 pixels, 12-bit, grey
442 values) using an industrial video camera (Flea, Point Grey Research, Vancouver, BC, Canada;
443 with a 25 mm lens, Cosmicar/Pentax). Both camera and hyperspectral sensor share the same

444 viewing orientation, but differ in their field of view (1° for the FieldSpec device and 10.5° for
445 the video camera).

446 Data from the FieldSpec hyperspectral instrument are currently being processed according to
447 the principle of Fraunhofer Line Discrimination. The same protocol for ground based and
448 airborne data is used to test for the influence of atmospheric absorption and to establish a
449 consistent data processing line from the canopy to the ecosystem level.

450

451 2.3.3 Regional mapping with the Airborne Hyperspectral Scanner (AHS)

452 The Airborne Hyperspectral Scanner (AHS) is an 80-bands airborne imaging radiometer (Fig.
453 3E), developed and built by SensyTech Inc., (currently Argon ST, and formerly Daedalus Ent.
454 Inc.) and operated by the Spanish Institute for Aerospace Technology (INTA) in different
455 remote sensing projects. It has 63 bands in the reflective part of the electromagnetic spectrum,
456 7 bands in the 3 to 5 μm range and 10 bands in the 8 to 13 μm region.

457 The AHS was first flown by INTA on September 2003. During 2004 the instrument was
458 validated during a number of flight campaigns which included extensive ground surveys
459 (SPARC-2004 and others), and is fully operational in INTA's C-212-200 EC-DUQ
460 "Paternina" aircraft since beginning of 2005 (Fig. 3D). AHS has been configured with distinct
461 spectral performances depending on the spectral region considered. In the VIS/NIR range,
462 bands are relatively broad (28 - 30 nm): the coverage is continuous from 0.43 up to 1.0 μm. In
463 the SWIR range, there is an isolated band centred at 1.6 μm with 90 nm width, simulate
464 corresponding band in satellite missions.

465 Next, there is a set of continuous, fairly narrow bands (18-19 nm) between 1.9 and 2.5 μm,
466 which are well suited for soil/geologic studies. In the MWIR and LWIR regions, spectral
467 resolution is about 300 to 500 nm, and the infrared atmospheric windows (from 3 to 5 μm and
468 from 8 to 13 μm) are fully covered. These spectral features allow to state that AHS is best
469 suited for multipurpose studies/campaigns, in which a wide range of spectral regions
470 including thermal have to be covered simultaneously.

471

2.3.4 First regional map of fluorescence derived from HYPER airborne imager

SIM.GA HYPER is a $512 + 256$-spectral-band push-broom sensor with VNIR and SWIR imaging capability. The instrument was provided by Galileo Avionica. The airborne hyperspectral system covers the 400-2450 nm spectral region and was operated at 1000 m. The hyperspectral HYPER SIM.GA is composed of two optical heads (Fig. 3F):

1) VNIR Spectrometer with a spectral range of 400-1000 nm, 512 spectral bands with 1.2 nm spectral sampling, 1024 spatial pixels across a swath of 722 m, which corresponds to a pixel resolution of 0.7×0.7 m

2) SWIR Spectrometer with a spectral range of 1000-2450 nm, 256 spectral bands with 5.8 nm spectral sampling, 320 spatial pixels across a swath of 425 m, which corresponds to a pixel resolution of 1.33×1.33 m

The optical heads are managed by a common data acquisition and control electronics. The HYPER SIM.GA works as a push-broom imager. A spatial line is acquired at nadir and the image is made exploiting the aircraft movement. The optical head of HYPER SIM.GA is rigidly coupled to a GPS/INS unit that collects data about platform movements (yaw, roll, pitch, velocity, altitude, lat, long) allowing to geo-rectify the images acquired. The use of GPS/INS unit reduces the mass and the cost of the instrument avoiding stabilized platform.

These campaigns were the first employment of this new airborne hyperspectral instrument and we are currently establishing the processing routines for geometrical and radiometrical processing of the data. With this communication we present the first results, automated routines allowing the processing of the extensive data sets are currently developed.

3 Selected first results highlighting the dynamics of variations in photosynthetic energy conversion

3.1 Leaf-level: Quantifying photosynthesis and fluorescence

3.1.1 Diurnal variations of photosynthetic efficiency

During the September campaign main focus was put on characterizing corn in the diurnal course. Leaf-level measurements showed a physiological limitation of photosynthesis during

different times of the day. Photosynthetic efficiency was high during environmentally moderate morning hours, a clear depression of photosynthetic efficiency was obvious during afternoon, when conditions were dry and hot, and photosynthetic efficiency increased again towards the evening, when conditions again became moderate. Diurnal courses of sun-induced fluorescence yield of corn were derived from spectrometric measurements and their potential as proxies for LUE was investigated. GPP was modeled using Monteith`s LUE-concept (Monteith, 1971, 1973) and GPP and LUE values were compared to synoptically acquired eddy covariance data. The diurnal response of complex physiological regulation of photosynthesis could be tracked from sun-induced fluorescence. Considering structural and physiological effects, this study showed for the first time that including sun-induced fluorescence improves modeling of diurnal courses of GPP. A detailed publication on this study is submitted (Damm et al, submitted).

3.1.2 Activation of photosynthesis within days

During the April campaign special focus was put on winter wheat that was a main crop in the study area. Weather conditions at the beginning of the campaign were wet and cloudy and photosynthesis of the plants was adapted to the low light and moderate conditions. Midday 18 April, 2007 weather changed and the whole region was abruptly exposed to longer lasting high pressure conditions with concomitant clear skies and warm and dry air.

This poses good conditions for a test case: Photosynthesis of the formerly low-light adapted plants had to acclimate to the now high light conditions. This was a specific advantage to test if these dynamic physiological changes were reflected in sun-induced fluorescence.

PAM fluorometry was used to analyze changes in photosynthetic activity and condition of photosynthetic apparatus of winter wheat plants. Among other parameters, ETR of photosystem II, non-photochemical quenching (NPQ) and steady-state fluorescence were determined. To relate these three parameters, the variation of these parameters at saturating light intensities was investigated in detail. Plants increased their ETR in the course of acclimation to the high light period. The increase was strongest in the morning. However, acclimation was associated with increasing leaf temperatures. At the beginning of the improved weather conditions, the NPQ at saturating light intensities was lowest around midday, but increased with the days in high light conditions. Concomitantly a slight decrease

in potential quantum efficiency was observed. This could be the sign of photoinhibition or of activation of sustained photoprotection mechanisms, due to high light intensities over the days. In contrast, steady-state fluorescence showed an inverse behaviour. The relation of fluorescence with non-photochemical quenching revealed a clear negative correlation, whereas fluorescence and ETR apparently were not correlated. No obvious correlation between NPQ and fluorescence with leaf temperature was observed. This suggests that fluorescence indeed is associated with properties describing the physiological status of photosynthesis and thus, may serve as a remote sensing measure to quantify changes of the efficiency of photosynthesis that occur on the relevant time scales. A detailed study of this topic will be published soon.

3.1.3 Characterization of sun-induced fluorescence emission spectrum at the leaf level

The shape of the fluorescence emission spectrum at the leaf level depends on many different parameters, such as the excitation wavelength, light intensity, pigment concentration or leaf structure. Fig. 4 compares sun-induced fluorescence emission spectra of leaves from different species under the same conditions of illumination (about 1700 μmol m^{-2} s^{-1}). It can be seen that leaves with the same chlorophyll content can show different emission spectra (e.g. wheat and bean). The shape parameters of the fluorescence emission spectrum are introduced into the retrieval algorithm of fluorescence from airborne data.

< figure 4>

3.2 Canopy-level

Ground-based diurnal cycles of sun- and laser-induced canopy fluorescence were collected with the aim of characterizing the temporal dynamic of fluorescence in addition to the spatial variation captured by airborne sensors (Section 3.3).

3.2.1 Variations of sun-induced canopy fluorescence

Diurnal cycles of canopy sun-induced fluorescence were collected during both the April and September campaigns over natural grassland (Velvetgrass), winter wheat and corn, respectively.

The diurnal cycle of both fluorescence fluxes (F687 at 687 nm and F760 at 760 nm) and Photosynthetic Active Radiation (PAR) during a sunny day is shown in Fig. 5A (21 April, 2007) but similar results are obtained for other days (Fig. 5B). One may observe that F687 closely followed PAR whereas less diurnal variation was observed on F760. It is hypothesized that this difference, already observed in other experiments (Louis et al. 2005), is due to a canopy structure effect. Nevertheless the fluorescence ratio F687/F760 was calculated and compared with the same ratio calculated for the in board AirFLEX data (Table 1). On-board data were processed to retrieve the fluorescence flux at the ground level after atmospheric corrections, according to Daumard et al (2007). Between 11:27 and 14:05, time of the airplane overpass, an increase of similar amplitude was observed on both on-board and ground measurements.

< Table 1 >

As another example, the diurnal variation of Fs at 760nm over winter wheat, measured at three days (22-24 April) under comparable meteorological conditions (i.e. clear sky) is shown in Figure 5B. As it is generally observed for photosynthesis, Fs exhibited a diurnal variation which is partially driven by incident PPFD (i.e. the more photons are absorbed, the more are dissipated through Fs). However, while PPFD showed a symmetrical trend around solar noon, Fs reached its maximum before solar noon (about 12:00 UTC) and decreased after 13:00 UTC. This trend was more easily observable with the Normalized Fs (Fs yield, Figure 5C) which is the yield of Fs per unit incident radiation (Meroni and Colombo, 2006). The diurnal course of Fs yield, which is expected to track the canopy LUE (e.g. Meroni et al., 2008), showed an increase during early morning, a depression during solar noon when the PPFD reached its maximum, followed by a recover in late afternoon.

< Figure 5 >

592

3.2.2 Variations of sun-induced canopy fluorescence over different agricultural crops

Main focus of this analysis was to investigate the variability of sun-induced fluorescence within the same field, of the same crop, and in different canopies. Additionally, the interdependency between Fs and the well established Normalized Difference Vegetation Index (NDVI) was investigated. The measured crop types and surface classes provide a high gradient of canopy structural parameters and the plant physiological status.

A first relative evaluation of the data showed a hyperbolic relationship of the Fs signal and the NDVI (Fig. 6) for different crop types and surfaces. A clear difference in the intra- and inner-field variation was obvious for both parameters. Moreover, the sensitivity of both parameters differs especially at the boundaries of the parameter range. On the one hand, the classical vegetation index saturated in dense canopies (e.g. when LAI is higher than 4) at a value of 0.9, where Fs still provided a differentiation of values (e.g. for winter wheat). On the other, the NDVI showed a significant variability for non vegetated surface classes (e.g. bare soil or water), whereas Fs values were more consistent with values around 0 for such non vegetated surfaces. Given insights from these first experiments the focus of future analysis will be put on a differentiated view on the impact of structural and functional response to the acquired signal.

< Figure 6 >

3.2.3 Active laser induced fluorescence mapping

The corn fields investigated during the September campaign were characterized by a large variability in chlorophyll content within the canopy and heterogeneous chlorophyll concentrations along the longitudinal axis of single leaves. Consequently, the shape and intensity of the chlorophyll fluorescence spectra at leaf level were markedly dependent on the leaf position into the canopy (Fig. 7A) and on the part of the leaf measured (Fig. 7B), in accordance with the well-known relationship between chlorophyll content and fluorescence reabsortion at the red fluorescence band (Buschmann, 2007). Therefore, the fluorescence

622   spectrum of the canopy was the result of heterogeneous contributions from the top layers as

623   well as of those coming from the inner layers, which underwent multiple reabsorption

624   processes.

625

626   < Figure 7 >

627

628   An example of a laser induced fluorescence (LIF) mapping for a corn canopy is shown in Fig.

629   8. The LIF measurements were performed by the FLIDAR system that covered a 1 m^2 area

630   (specifically, the area was about 80 x 120 cm) of the corn field within small angles from nadir

631   (Fig. 8A). The spot effectively measured with the FLIDAR system at each laser pulse was a

632   circular area of 2.5 cm in diameter. The whole fluorescence spectrum between 580 and

633   830 nm was recorded for each spot. The spatial resolution, defined as the distance between

634   the center of one measured spot and the next one, was about 4.5 cm both in the vertical and

635   horizontal direction. The images consist of 18 x 27 pixels and each pixel value corresponds to

636   the integral of the fluorescence spectrum, obtained as an average of 20 spectral measurements

637   with 532 nm excitation, in the 760 nm $\pm$ 2.5 nm band. Measurements with very low

638   fluorescence intensity at 680 nm (e.g. soil or dried vegetation) were marked as black pixels to

639   exclude them from further analysis.

640   As expected, the fluorescence map was found to be largely heterogeneous. Although it was

641   difficult to appreciate significant changes in the fluorescence evolution over the day, a general

642   decrease of the F760 nm signal appeared (Fig. 8B-D). This variation was confirmed by the

643   fluorescence signal, determined as average over the canopy area. As shown in Fif 9A, the

644   fluorescence signals decreased in a magnitude of 15% from 08:00 to 15:00 CET. Similar

645   results were obtained for a second diurnal course of the same corn canopy recorded on 15

646   September, 2007 (data not shown).

647

648   < Figure 8 >

649

3.2.4 Comparison between Sun Induced Fluorescence and Laser Induced Fluorescence

The comparison between Sun Induced Fluorescence (SIF) and Laser Induced Fluorescence (LIF) measurements at the canopy level is important to better understand variation of SIF within days and seasons. Furthermore, only few data sets concerning the relationship between active and passive chlorophyll fluorescence are reported into the literature (Moya et al. 2004; Liu et al. 2005; Pérez-Priego et al. 2005). In those studies, the active measurements were restricted to the leaf level, hence, they were limited for calibration purposes of canopy related SIF measurements.

In this study, canopy LIF data were compared to SIF data, which were acquired as described in section 2.2.2. LIF-measurements were done within the same corn field in Marmande, at the same time but in a distance of few tenths of meters to the SIF-measuremets. Some corn plants were selected next to the control area and the water flow was interrupted by cutting their stem. The plants were fixated with poles to keep their original position.

The time courses of the normalized SIF signal at 760 nm and of the LIF signal measured at the same wavelength is shown in Figure 9A for both the control and treated areas (stem cutting occurred at 9:30). In general, both SIF and LIF signals of the control canopies showed a trend to decrease with time. The decrease in the SIF was less evident, but still visible. This discrepancy is rather small considering the difference in the excitation light (wavelength and intensity) and in the excitation/detection geometry of the two measuring systems. The passive fluorescence data were largely dependent on the solar-zenith angle that affects penetration of the excitation light into the canopy. Consequently, the contributions from leaves in the inner layers to the fluorescence signal can change with time and may not be adequately normalized by using the solar radiation incident on the horizontal plane. On the contrary, in the LIF measurements, the excitation/detection geometry was constant.

< Figure 9 >

The average light intensity of the laser excitation at 532 nm was always less than half the incident solar PAR measured during the experiment (1100-1500 μmol m^{-2}s^{-1}), therefore, no

680   marked perturbation of the leaf photosynthetic state was expected to be induced by the
681   excitation beam.

682   Under desiccation stress, both LIF and SIF values showed a larger decrease during the day
683   with respect to the controls (Fig. 9A). This trend was more evident in the ratio between
684   control and stressed plant fluorescence signals (Fig. 9B). For both techniques, the difference
685   in fluorescence between control and stressed plants increased with time.

686

687

688   **3.3   Regional level**

689   3.3.1 Repeated transects using AirFLEX

690   Repeated transects using AirFLEX have been performed over an area of about 130 km by
691   80 km covered with various vegetation types such as winter wheat, corn, vineyard, fruit trees,
692   grassland, oak forest, pine forest and also bare fields which are useful for calibration purpose.
693   Fig. 10 shows a map of these transects over some of the Marmande test fields (top). It also
694   shows the corresponding fluorescence signals as well as the Normalized Difference
695   Vegetation Index (NDVI) over three different fields covered with corn and bean (bottom).
696   One can see a significant increase of NDVI between the first corn field and the bean field,
697   while there were only little changes between the bean field and the second corn field. These
698   observations could be related to the senescence of the first corn field that was observed from
699   the video images (data not shown). It can be seen from Fig. 10B that many fluorescence
700   variations were correlated to NVDI variations. However, larger variations were observed on
701   fluorescence signals. Fluorescence also showed variations from field to field that could not be
702   explained by NDVI changes. It was the case of the F687 signal when going from the bean
703   field to the second corn field. These fluorescence changes were most probably related to
704   different canopy structure, as bean is a dicot with a rather planophile structure while corn is a
705   monocot having a more erectophile structure. Similar results have been already reported in
706   Moya et al (2006).

707

708   < Figure 10 >

24

709

710 To investigate spatial and temporal variability of fluorescence signals at a wider spatial scale,
711 an analysis based on a number of target fields along the flight track was performed. Portions
712 of land belonging to specific land use and land cover classes were identified and
713 parameterized, by visual inspection of the video images acquired during the flights. Each field
714 was marked and basic statistical computations were computed from the fluorescence signal.
715 In total, 40 fields were identified over pine forest, and 42 over winter wheat land uses, besides
716 smaller amounts of fields over other land use classes. Fields had similar and homogeneous
717 characteristics, in terms of texture and NDVI. Mean NDVI was computed from the flights is
718 0.83 ± 0.07 over pine and 0.87 ± 0.08 over wheat. Not all the fields were sampled in all the
719 flights, because of track variations between different flights. Nevertheless, investigating the
720 aggregated fluorescence response over these fields can provide information on the spatial and
721 temporal variability of the observations, and on the absolute magnitudes of fluorescence
722 signals at a wider scale with respect to point observations. Fig. 11 shows the diurnal course of
723 the fluorescence flux over pine and wheat fields respectively, together with incoming PPFD.
724 Variability related to differences between fields is encompassed by vertical deviation bars.
725 Both fluorescence signals showed a diurnal shape that obviously was driven by incoming
726 radiation, but important differences in fluorescence signals over different land cover exist;
727 fluorescence was on average 53% higher on wheat then on pine forest, while corresponding
728 average incoming PPFD, as directly measured at the time of observations, did not show any
729 remarkable difference. Even in absence of direct canopy-scale LUE measurements over target
730 fields, LUE of a fast developing winter wheat canopy in April was expected to be higher than
731 LUE over mature pine forests, suggesting that Fs can potentially explain LUE spatial
732 variability when compared at different areas. The influences and the relative importance of
733 structural effects on the fluorescence radiometric signals are not yet well known and may play
734 a role in explaining part of this observed variability.

735

736 < Figure 11 >

737

3.3.2 First regional map of fluorescence derived from HYPER airborne imager

The spatial analysis of the fluorescence signal by means of imaging spectroscopy data is complex. The signal recorded by airborne line scanners with a relatively large field-of-view varies strongly across the track, i.e. perpendicular to the flight direction, due to a variety of disturbing effects (e.g. Kennedy et al, 1997, Schiefer et al, 2006). With regard to the derivation of the fluorescence signal the following effects have to be considered: (1) data from push-broom sensors like HYPER are influenced by shifts in the position and width of spectral bands. This view-angle variation is known as "smile effect"; (2) atmospheric scattering in the NIR regions vary with path length between sensor and Earth surface and increases towards larger view-angles; (3) anisotropic surface reflectance that are a function of the fractions of sunlit and shaded surfaces are driven by the direction of incoming solar irradiance and position of the sensor (Pinty et al., 2002). All these effects require special attention when the raw data is transferred into surface reflectance and a normalization of such effects has to be included into radiometric calibration and atmospheric correction. Moreover, knowledge on the directionality of the fluorescence signal as emitted by canopies is still very limited and possible influences cannot be estimated at the moment.

First attempts to compute reliable reflectance values from the HYPER images showed a high degree of statistical noise and problems with the radiometric calibration because of bad pixels and uneven radiometric response of the sensor. The across track gradients caused be the smile effect appear to be dominant (Fig. 12, top). Therefore, it was not feasible to derive fluorescence in physical values. As alternative we used an empirical normalization to account for most of the disturbing effects and relative fluorescence values. This empirical normalization used the fact, that the across track effects also exist in soil data, which may be used as reference during the FLD method. For normalization bare soil surfaces were manually selected in the image. The spectral information from these soil surfaces was then used to derive an average soil signal for each viewing angle. By incorporating this varying signal, the FLD was set up as a function of view angle and normalized fluorescence values were derived for the entire image. In doing so, the requirement of the reference signal being viewed under identical illumination conditions as the target signal (Moya et al, 2004) was met. However, differences in the directional behaviour of soils and vegetation, as well as knowledge gaps on the directionality of emitted fluorescence limit the accuracy and an evaluation of absolute fluorescence value is not feasible with this empirical approach.

26

770 Nevertheless, it was possible to evaluate the spatial distribution of fluorescence and to achieve

771 first insights on the spatial variations of fluorescence (Fig. 12, bottom). Clear differences in

772 intra- and inner-field variation of the fluorescence signal were observed for agricultural areas

773 near Marmande. Differences correlate to some extent with traditional index-based proxies for

774 vegetation or with vegetation fractions derived from spectral mixture analyses. However, such

775 index-based measures often saturate at values where fluorescence still allows differentiating

776 photosynthetic activity. Moreover, the absolute fluorescence signal differed clearly between

777 different crop types having the same leaf area, providing information that cannot be derived

778 by traditional measures.

779

780   < figure 12 >

781

782

783 **4   Conclusions**

784 Current satellite remote sensing techniques do not have the potential to quantify the actual

785 status of photosynthetic light conversion and light use efficiency (LUE) is thus not

786 implemented as an operational input parameter in current carbon models. The fluorescence

787 signal is to date the most power full signal that is directly related to actual photosynthetic

788 efficiency. With this paper we demonstrated the potential, but also the open questions to

789 measure fluorescence from the leaf to the mesoscale. We also showed a path how this directly

790 measured signal can be used for a better estimate of leaf and ecosystem carbon fixation and

791 potentially evapotranspiration. Several campaigns and scientific studies are currently under

792 way to better understand the link between sun-induced fluorescence and variations in

793 photosynthetic carbon fixation and to explore the technical feasibility to detect the signal

794 accurately from a space born platform. These conditions were strongly supported by the

795 FLEX mission as one of ESA's candidate missions for a future Earth Explorer (Rascher,

796 2007). Fluorescence definitely shows potential as a direct measure of actual photosynthesis,

797 nevertheless, we do not underestimate the challenges especially that of scaling up leaf-level

798 methods to the canopy level. The plant canopy is a complex three-dimensional structure that

799 changes due to environmental factors and structural adaptations of the plants.

800

801

Acknowledgements

812

References

813   **References**

814   Alonso, L., Gómez-Chova, L., Vila-Francés, J., Amorós-López, J., Guanter, L., Calpe, J., and

815   Moreno, J.: Improved Fraunhofer Line Discrimination method for vegetation fluorescence

816   quantification., IEEE Geoscience and Remote Sensing Letters, 5, 620-624, 2008.

817   Bilger, W., Schreiber, U., and Bock, M.: Determination of the quantum efficiency of

818   photosystem II and of non-photochemical quenching of chlorophyll fluorescence in the field,

819   Oecologia, 102, 425-432, 1995.

820   Buschmann, C.: Variability and application of the chlorophyll fluorescence emission ratio

821   red/far-red of leaves., Photosynthesis Research, 92, 261-271, 2007.

822   Corp, L. A., Middleton, E. M., McMurtrey, J. E., Entcheva Campbell, P. K., and Butcher, L.

823   M.: Fluorescence sensing techniques for vegetation assessment, Applied Optics, 45, 1023-

824   1033, 2006.

825   Damm, A., Elbers, J., Erler, A., Gioli, B., Hamdi, K., Hutjes, R., Kosvancova, M., Meroni,

826   M., Miglietta, F., Moersch, A., Moreno, J., Schickling, A., Sonnenschein, R., Udelhoven, T.,

827   van der Linden, S., van der Tol, C., Hostert, P., and Rascher, U.: Remote sensing of sun

828   induced fluorescence to improve modelling of diurnal courses of gross primary productivity

829   (GPP), Global Change Biology, submitted.

830   Daumard, F., Goulas, Y., Ounis, A., Pedros, R. and Moya, I.: Atmospheric correction of

831   airborne passive measurements of fluorescence, in: ISPMSRS07, Davos, Switzerland, 12-14

832   March   2007,   P58,   available   at:

833   http://www.commission7.isprs.org/ispmsrs07/P58_Daumard_fluorescence.pdf, 2007.

834   Evain, S., Camenen, L., and Moya, I.: Three channels detector for remote sensing of

835   chlorophyll fluorescence and reflectance from vegetation, 8th international symposium:

836   Physical measurements and signatures in remote sensing, Aussois, France, 395-400, 2001.

837   Field, C. B., Randerson, J. T., and Malmstrom, C. M.: Global Net Primary Production -

838   Combining ecology and remote sensing, Remote Sensing of Environment, 51, 74-88, 1995.

839   Flexas, J., Briantais, J.-M., Cerovic, Z. G., Medrano, H., and Moya, I.: Steady-state and

840   maximum chlorophyll fluorescence responses to water stress in grapevine leaves: A new

841   remote sensing system, Remote Sensing of Environment, 73, 283-297, 2000.

842 Flexas, J., Escalona, J. M., Evain, S., Gulias, J., Moya, I., Osmond, C. B., and Medrano, H.:
843 Steady-state chlorophyll fluorescence (Fs) measurements as a tool to follow variations of net
844 CO_2 assimilation and stomatal conductance during water-stress in C3 plants, Physiologia
845 Plantarum, 114, 231-240, 2002.

846 Gamon, J.A.; J. Peñuelas, J.; and Field, C.B.: A narrow-waveband spectral index that tracks
847 diurnal changes in photosynthetic efficiency. Remote Sensing of Environment, 41. 35-44,
848 1992.

849 Goetz, S. J., and Prince, S. D.: Modelling terrestrial carbon exchange and storage: Evidence
850 and implications of functional convergence in light-use efficiency, Advances in Ecological
851 Research, 28, 57-92, 1999.

852 Gómez-Chova, L., Alonso, L., Amorós-López, J., Vila-Francés, J., del Valle-Tascón, S.,
853 Calpe, J., and Moreno, J.: Solar induced fluorescence measurements using a field
854 spectroradiometer. Earth Observation For Vegetation Monitoring And Water Management.,
855 AIP Conference Proceedings, 274-281, 2006.

856 Hilker, T., Coops, N. C., Wulder, M. A., Black, A. T., and Guy, R. D.: The use of remote
857 sensing in light use efficiency based models of gross primary production: A review of currant
858 status and future requirements, Science of the Total Environment, 404, 411-423, 2008.

859 Kennedy, R. E., Cohen, W. B., and Takao, G.: Empirical methods to compensate for a view-
860 angle-dependent brightness gradient in AVIRIS imagery, Remote Sensing of Environment,
861 62, 277-291, 1997.

862 Liu, L., Zhang, Y., Wang, J., and Zhao, C.: Detecting solar-induced chlorophyll fluorescence
863 from field radiance spectra based on the Fraunhofer Line Principle, IEEE Transactions on
864 Geosciences and Remote Sensing, 43, 827-832, 2005.

865 Louis, J., Ounis, A., Ducruet, J.-M., Evain, S., Laurila, T., Thum, T., Aurela, M., Wingsle, G.,
866 Alonso, L., Pedros, R., and Moya, I.: Remote sensing of sunlight-induced chlorophyll
867 fluorescence and reflectance of Scots pine in the boreal forest during spring recovery, Remote
868 Sensing of Environment, 96, 37-48, 2005.

869 Lucht, W., Barker Schaaf, C., and Strahler, A. H.: An algorithm for the retrieval of Albedo
870 from space using semiempirical BRDF models, IEEE Transactions on Geosciences and
871 Remote Sensing, 38, 977-998, 2000.

872 Maier, S., Günther, K. P., and Stellmes, M.: Sun-Induced Fluorescence: A new Tool for
873 Precision Farming, in: Digital Imaging and Spectral Techniques: Applications to Precision
874 Agriculture and Crop Physiology, edited by: VanToai, R., Major, D., McDonald, M.,
875 Schepers, J., and Tarpley, L., ASA Special Publications, Madison, Wisconsin, USA, 209-222,
876 2003.

877 Meroni, M., and Colombo, R.: Leaf level detection of solar induced chlorophyll fluorescence
878 by means of a subnanometer resolution spectroradiometer, Remote Sensing of Environment,
879 103, 438-448, 2006.

880 Meroni, M., Picchi, V., Rossini, M., Cogliati, S., Panigada, C., Nali, C., Lorenzini, G., and
881 Colombo, R.: Leaf level early assessment of ozone injuries by passive fluorescence and PRI,
882 International Journal of Remote Sensing, 29, 5409-5422, 2008.

883 Meroni, M., Rossini, M., Guanter, L., Alonso, L., Rascher, U., Colombo, R., and Moreno, J.:
884 Remote sensing of solar induced chlorophyll fluorescence: review of methods and
885 applications, Remote Sensing of Environment, submitted.

886 Middleton, E. M., Corp, L. A., and Entcheva Campbell, P. K.: Comparison of measurements
887 and FluorMOD simulations for solar-induced chlorophyll fluorescence and reflectance of a
888 corn crop under nitrogen treatments, International Journal of Remote Sensing, 29, 5193-5213,
889 2008.

890 Milton, E. J., and Rolling, E. M.: Estimating the irradiance spectrum from measurements in a
891 limited number of spectral bands, Remote Sensing of Environment, 100, 348-355, 2006.

892 Monteith, J. L.: Solar-radiation and productivity in tropical ecosystems, Journal of Applied
893 Ecology, 9, 747-766, 1972.

894 Monteith, J. L.: Climate and efficiency of crop production in Britain, Philosophical
895 Transactions of the Royal Society of London Series B-Biological Sciences, 281, 277-294,
896 1977.

897 Moya, I., Camenen, L., Latouche, G., Mauxion, C., Evain, S., and Cerovic, Z. G.: An
898 instrument for the measurement of sunlight excited plant fluorescence, in: Photosynthesis:
899 Mechanisms and Effects, edited by: Garab, G., Kluwer Academic Publishers, Dordrecht,
900 4265-4270, 1999.

Moya, I., Camenen, L., Evain, S., Goulas, Y., Cerovic, Z. G., Latouche, G., Flexas, J., and Ounis, A.: A new instrument for passive remote sensing. - 1. Measurements of sunlight-induced chlorophyll fluorescence, Remote Sensing of Environment, 91, 186-197, 2004.

Moya, I., Daumard, F., Moise, N., Ounis, A., Goulas, Y.: First airborne multiwavelength passive chlorophyll fluorescence measurements over La Mancha (Spain) fields, in: 2nd International Symposium on Recent Advances in Quantitative Remote Sensing (RAQRS II), Torent, Spain, 25-29 September 2006, 820-825, available at: http://www.uv.es/raqrs/index.pdf, 2006.

Neininger, B.: A small aircraft for more than just ozone: Metair's 'Dimona' after ten years of evolving development, Proceedings of the 11th Symposium on Meteorological Observations and Instrumentation, 81st AMS Annual Meeting, Albuquerque, NM, USA, 14-19 January 2001, 2001.

Papageorgiou, G. C., and Govindjee: Chlorophyll a Fluorescence: A Signature of Photosynthesis, Advances in Photosynthesis and Respiration, 19, Kluwer Academic Publications, Dordrecht, 2004.

Pérez-Priego, O., Zarco-Tejada, P. J., Miller, J. R., Sepulcre-Cantó, G., and Fereres, E.: Detection of Water Stress in Orchard Trees with a High-Resolution Spectrometer through Chlorophyll Fluorescence in-filling of the O2-A band, IEEE Transactions on Geosciences and Remote Sensing, 43, 2759-2769, 2005.

Pinty, B., Widlowski, J.-L., Gobron, N., Verstraete, M. M., and Diner, D. J.: Uniqueness of multiangular measurements — Part I: An indicator of subpixel surface heterogeneity from MISR, IEEE Transactions on Geosciences and Remote Sensing, 40, 1560-1573, 2002.

Plascyk, J. A.: MK II Fraunhofer Line Dicsriminator (FLD-II) for airborne and orbital remote-sensing of solar-stimulated luminescence, Optical Engineering, 14, 339-346, 1975.

Rascher, U., Liebig, M., and Lüttge, U.: Evaluation of instant light-response curves of chlorophyll-fluorescence parameters obtained with a portable chlorophyll fluorometer on site in the field, Plant, Cell & Environment, 23, 1397-1405, 2000.

Rascher, U., and Nedbal, L.: Dynamics of plant photosynthesis under fluctuating natural conditions, Current Opinion in Plant Biology, 9, 671-678, 2006.

930   Rascher, U.: FLEX - FLuorescence EXplorer: a remote sensing approach to quantify spatio-
931   temporal variations of photosynthetic efficiency from space, Photosynthesis Research, 91,
932   293-294, 2007.

933   Running, S. W., Thornton, P. E., Nemani, R., and Glassey, J. M.: Global terrestrial gross and
934   net primary productivity from the earth observing system, in: Methods in Ecosystem Science,
935   edited by: Sala, O. E., Jackson, R. B., Mooney, H. A., and Howarth, R. W., Springer Verlag,
936   New York, 44-57, 2000.

937   Schiefer, S., Hostert, P., and Damm, A.: Correcting brightness gradients in hyperspectral data
938   from urban areas, Remote Sensing of Environment, 101, 2006.

939   Schmitgen, S.; Geiß, H.; Ciais, P.; Neininger, B.; Brunet, Y.; Reichstein, M.; Kley, D.; and
940   Volz-Thomas, A.: Carbon dioxide uptake of a forested region in southwest France derived
941   from airborne CO_2 and CO measurements in a quasi-Lagrangian experiment. Journal of
942   Geophysical Research - Atmosphere, 109, D14, art. no. D14302, 2004.

943   Schulze, E. D., and Caldwell, M. M.: Ecophysiology of photosynthesis, Ecological Studies,
944   Springer, Berlin, Heidelberg, 1994.

945   Schurr, U., Walter, A., and Rascher, U.: Functional dynamics of plant growth and
946   photosynthesis – from steady-state to dynamics – from homogeneity to heterogeneity, Plant
947   Cell & Environment, 29, 340-352, 2006.

948   Turner, D. P., Ritts, W. D., Cohen, W. B., Gower, S. T., Zhao, M. S., Running, S. W., Wofsy,
949   S. C., Urbanski, S., Dunn, A. L., and Munger, J. W.: Scaling Gross Primary Production (GPP)
950   over boreal and deciduous forest landscapes in support of MODIS GPP product validation,
951   Remote Sensing of Environment, 88, 256-270, 2003a.

952   Turner, D. P., Urbanski, S., Bremer, D., Wofsy, S. C., Meyers, T., Gower, S. T., and Gregory,
953   M.: A cross-biome comparison of daily light use efficiency for gross primary production,
954   Global Change Biology, 9, 383-395, 2003b.

955

956 **Tables**

957 Table 1 Simultaneous measurement of the F687/F760 ratio from the airborn AirFLEX sensor

958 and on ground.

Date	Time (UTM)	NDVI Plane	F687/F760 Plane (AirFLEX)	F687/F760 Ground (SpectroFLEX)	NDVI Ground
21/04/2007	11:27	0.81	1.82 ± 0.7	1.44 ± 0.35	0.74
21/04/2007	14:05	0.78	2.11± 0.7	1.76 ± 0.35	0.68

959

960

961
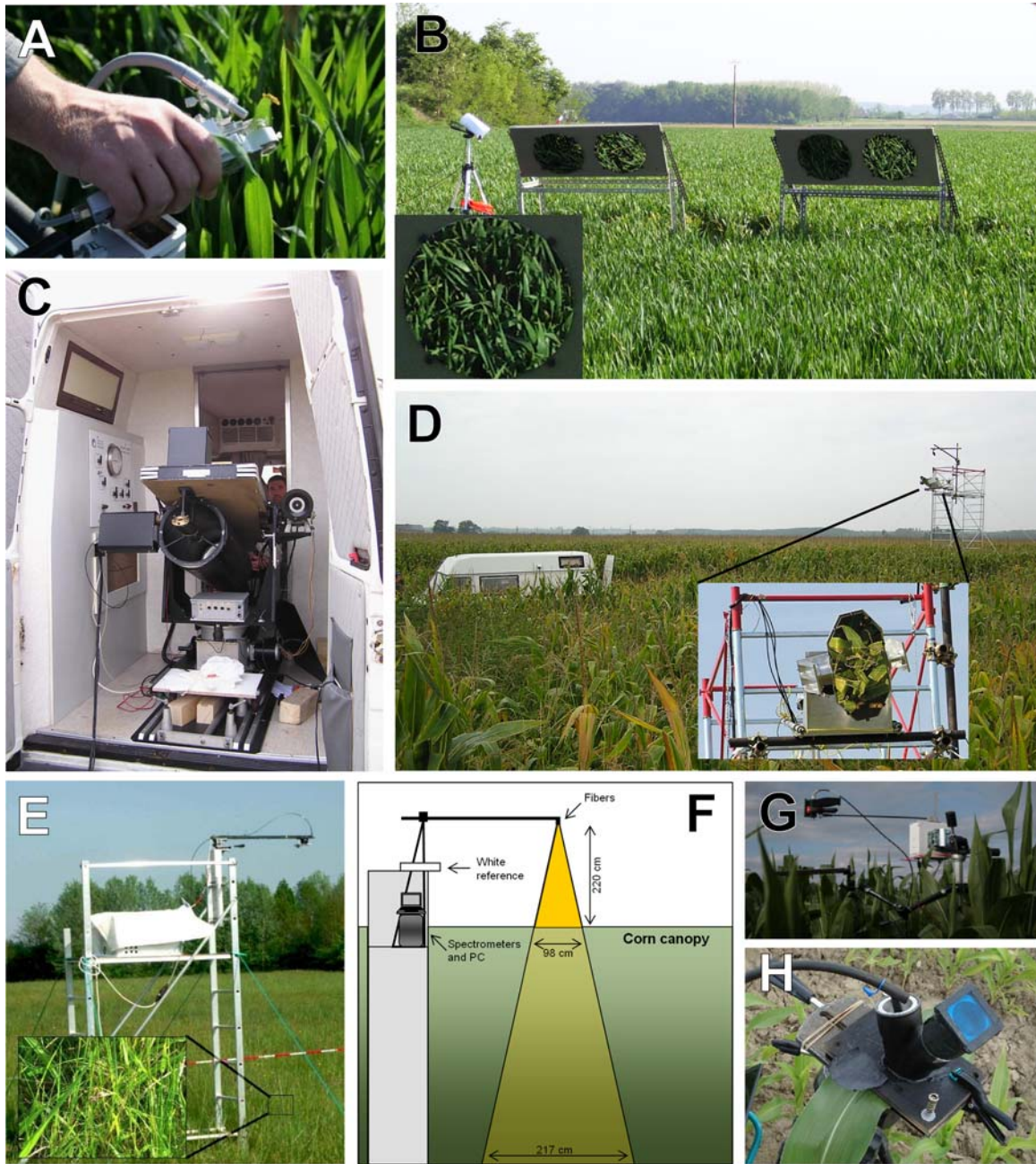
Figures

Figure 1. Ground measurement set-up to quantify changes of photosynthetic efficiency from the leaf to the canopy level. A: Mini-PAM measurement within winter wheat. Fluorescence emission and photosynthetic quantum efficiency is characterized with this fast screening method at hundreds of representative leaves under the prevailing environmental conditions. B: Mirror set-up of the active FLIDAR imaging system as they were installed in April in winter wheat. C: FLIDAR imaging system of the group of G. Agati. The laser system was installed

971   inside a van variably targeting mirrors in the field. D: computer controlled movable mirror of

972   the active FLIDAR imaging system as they were installed in September a few meters above a

973   corn canopy. E: The SpectroFLEX set up for passive fluorescence measurements in the O_2-B

974   (687 nm) and O_2-A (760 nm) bands. The number of bands, widths and central wavelengths

975   have been chosen similar to those of the AirFLEX airborne sensor. The scaffolding was in the

976   middle of a large grassland field in which several acquisition points by the AirFLEX sensor

977   were possible. The target was Velvetgrass (*Holcus Lanatus)*, an erectophile monocot species

978   of about 60 cm height. The averaged chlorophyll concentration was 27 µg cm^{-2}. F: Schematic

979   drawing of the passive measurements set-up (1) in chapter 2.2.2. G: Spectrometric set-up (3)

980   explained in chapter 2.2.2. An automated arm constantly moved the fibre optics of a

981   FieldSpec system between the reflectance standard and three spots of vegetation. Installation

982   above corn in September. The same, cross-calibrated detector was used airborne (Fig. 3A). H:

983   Spectrofluorometer for measurement of sun-induced fluorescence emission spectra.

984
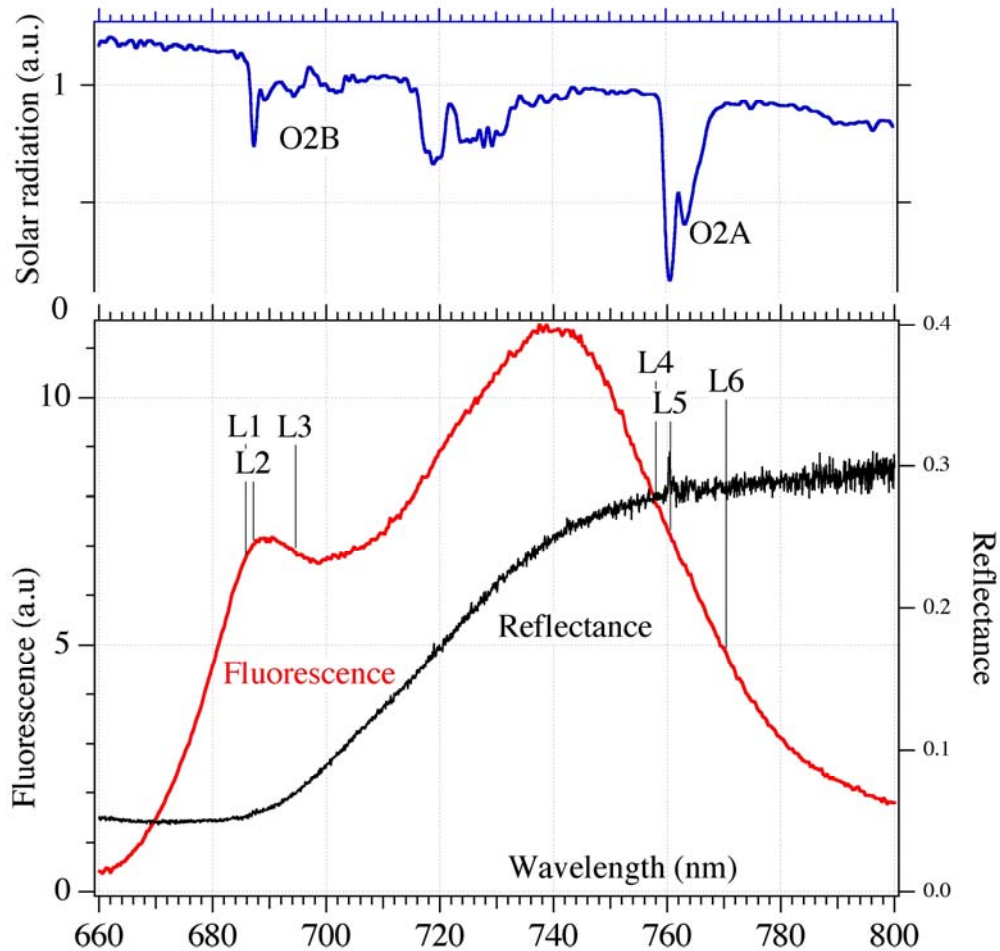
Figure 2. Top. Solar spectrum showing the O_2 bands at the spectral resolution of the AirFLEX sensor. Bottom. Red and near-infrared region of the fluorescence emission spectrum after full sun light adaptation of a Velvetgrass leaf. Sun-induced fluorescence was measured with the special instrument described in 2.1.3. The reflectance spectra has been superimposed. It was acquired at the canopy level with the SpectroFLEX set-up. The positions of the central wavelengths (Li) of the six channels of the AirFLEX sensor are also shown. These spectra were required to retrieve the fluorescence by the FLD principle.
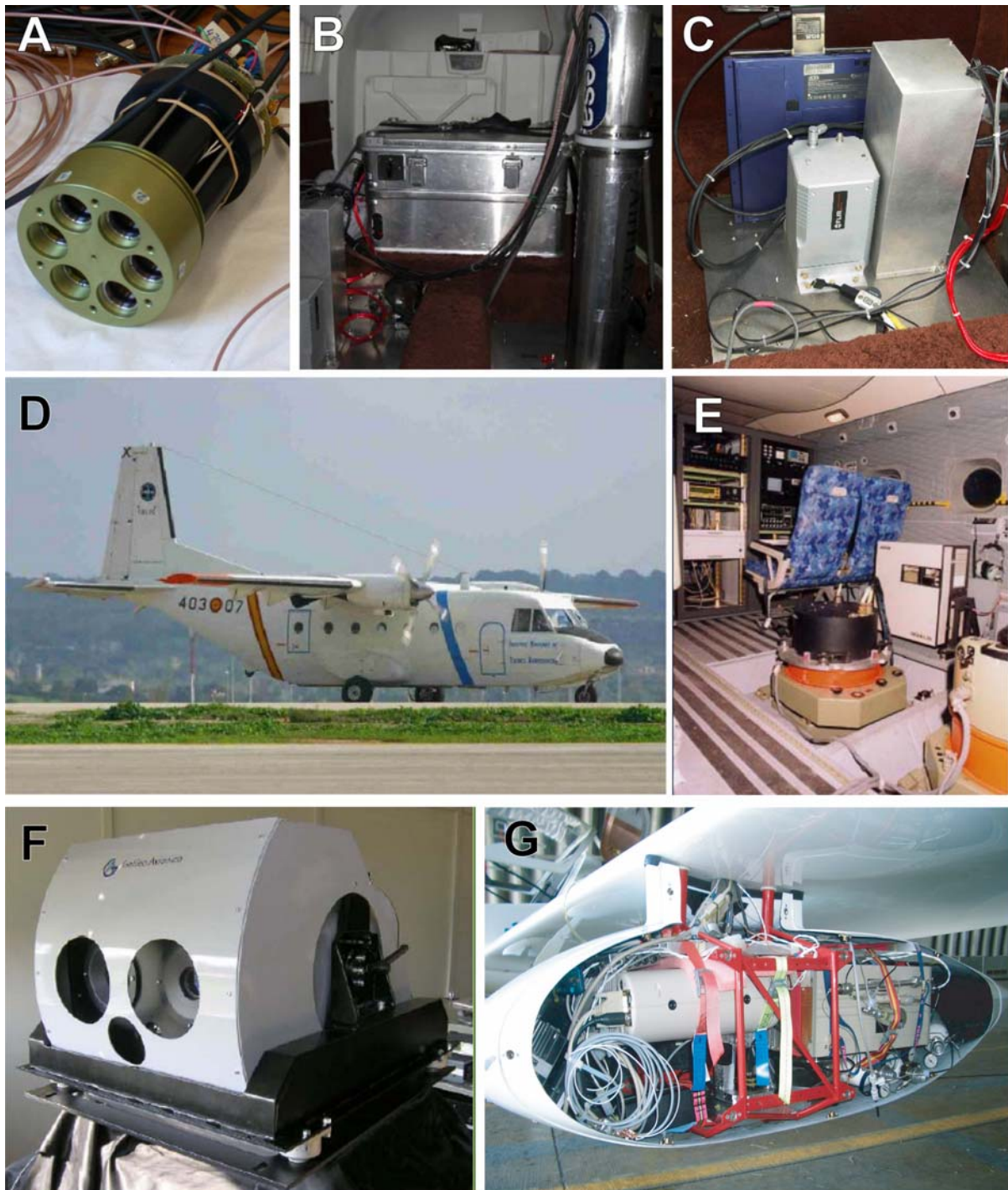
Figure 3. Airborne instruments that were employed during the campaign to quantify changes of photosynthetic efficiency from the field to the regional level. A: Internal sensor head of the AirFLEX sensor showing the six channels for O_2-A and O_2-B fluorescence retrieval. Each channel requires three spectral bands: within the atmospheric absorption feature and on the

1001   left and right shoulder of the absorption feature. B: Picture of AirFLEX installed on board the

1002   CNR SENECA during the campaigns. C: Thermal camera on board the SENECA. D: INTA

1003   C-212-200 EC-DUQ "Paternina" aircraft. Within this aircraft both the AHS and HYPER

1004   sensor were installed for parallel recording of flight lines. E: AHS hyperspectral imager

1005   onboard EC-DUQ "CASA" as arranged during the CEFLES 2 campaign. F: Picture of the

1006   SIM.GA HYPER sensor, which was first time used during the CEFLES2 campaign. G:

1007   Underwing pod with the FieldSpec hyperspectral reflectance instrument. The instrument

1008   continuously acquired spectra with 2Hz resolution along repeated overpasses during the

1009   campaign. The same, cross-calibrated detector was used on the ground (Fig. 1H).

1010
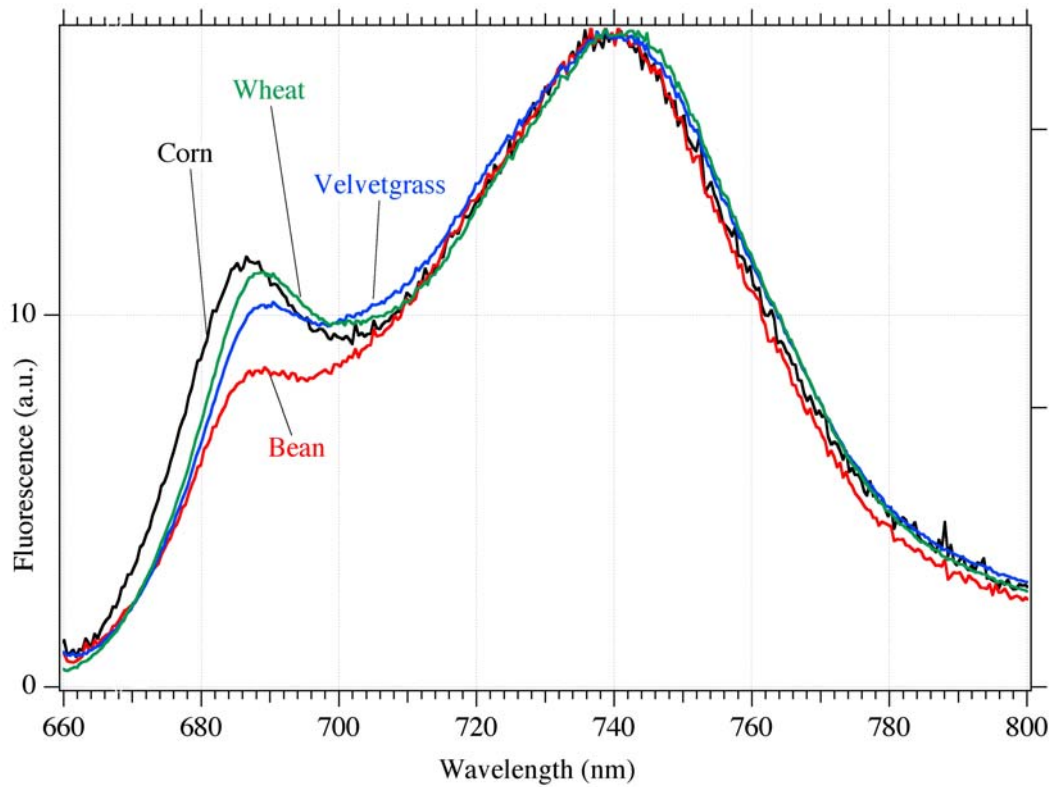
1011

1012

1013 Figure 4: Variability of sun-induced fluorescence emission spectra after light adaptation

1014 (1700 μmol photons m^{-2} s^{-1}). Adaxial sides of leaves from four species were measured with

1015 the special instrument described in 2.1.3. Chlorophyll content (μg cm^{-2}): Corn 48, Bean 42.2,

1016 Velvetgrass 27.1.Wheat 41.9.

1017
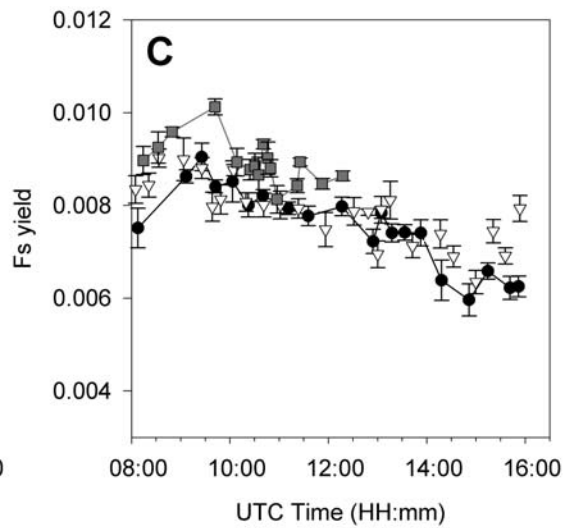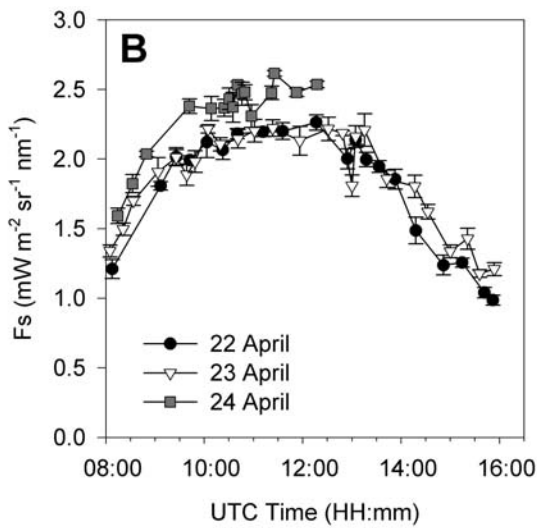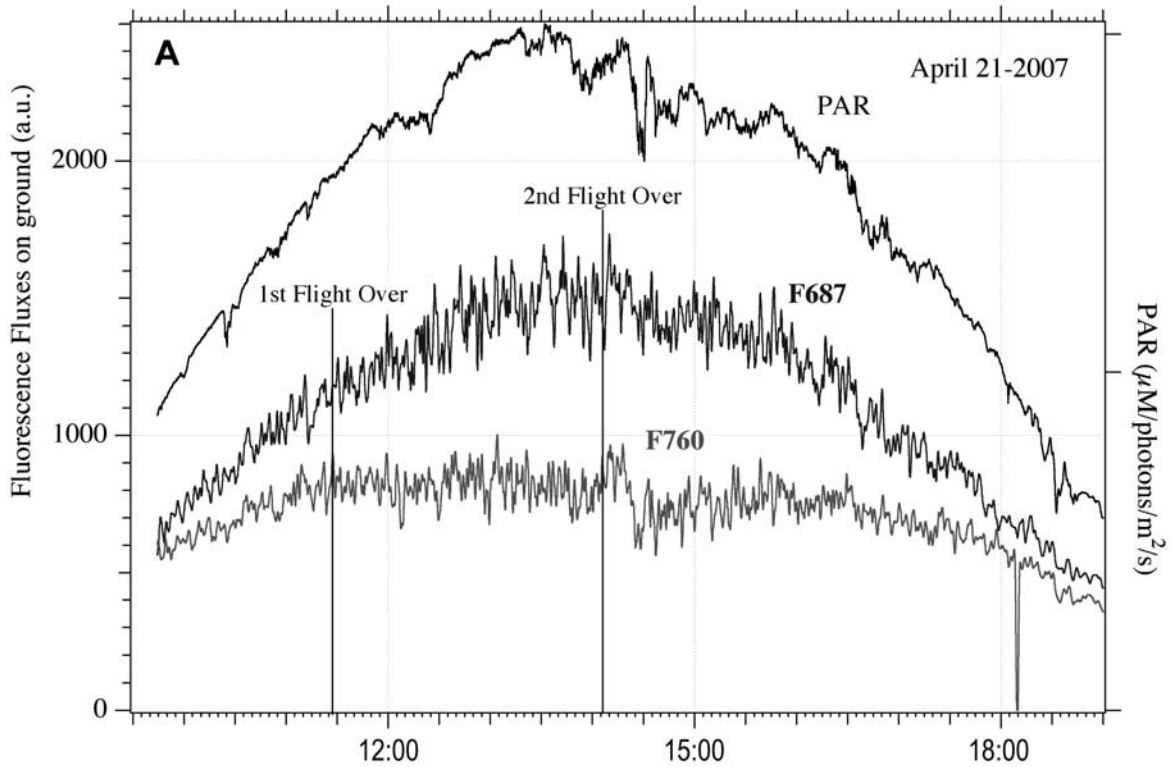
Figure 5. (A): Diurnal course of fluorescence fluxes at 687 and 760 nm, (F687 and F760) and Photosynthetic Active Radiation (PAR), measured at the canopy level with the SpectroFLEX set-up. Similar results were obtained on 22 and 23 April, 2007. Vertical black lines indicates the moment at which the field has been flight over. The fluorescence ratios inboard and at ground level are compared in Table2. B, C: Diurnal courses of sun-induced fluorescence (Fs) and normalized Fs (Fs yield) at 760 nm measured over three measurement days. Values represent mean ± SE (n = 4 consecutive measurements). Measurements were collected over a

1027   winter wheat dense canopy (LAI = 6.3 $m^2 m^{-2}$) during three days of measurements (22-24

1028   April, 2007) at the Marmande main site.

1029
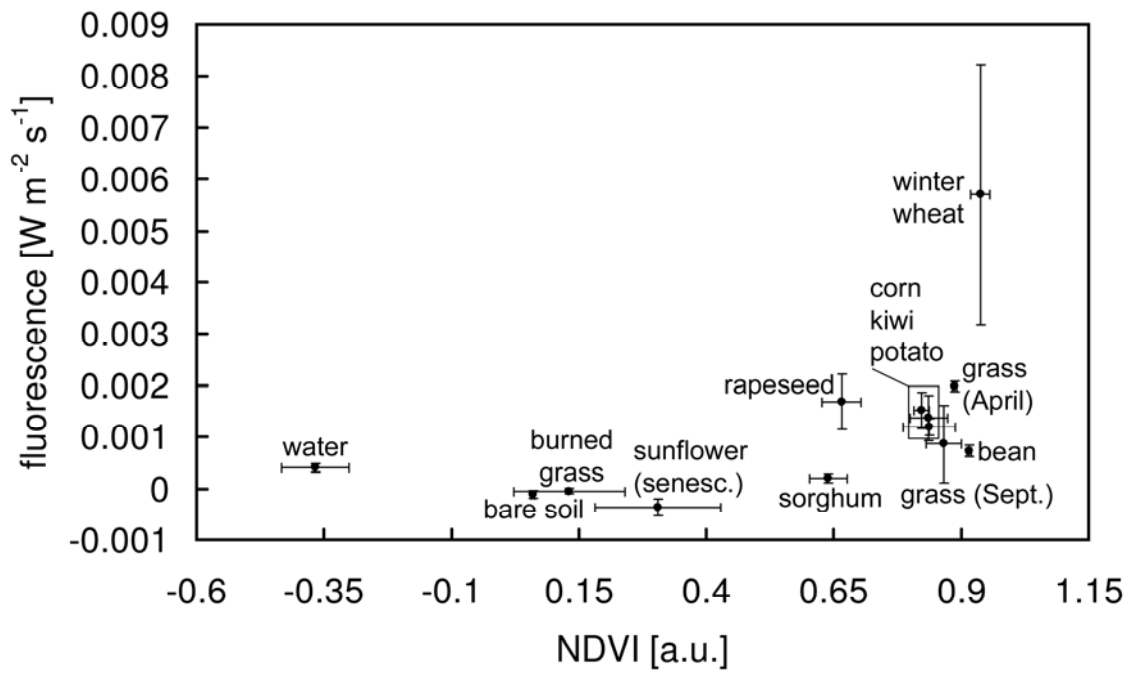
1030

1031

1032   Figure 6. Sun-induced fluorescence and NDVI over different 11 agricultural crops and two

1033   additional surface classes. For each canopy type, average and standard deviation of 12 single

1034   measurements were calculated (winter wheat 84, corn 96).

1035
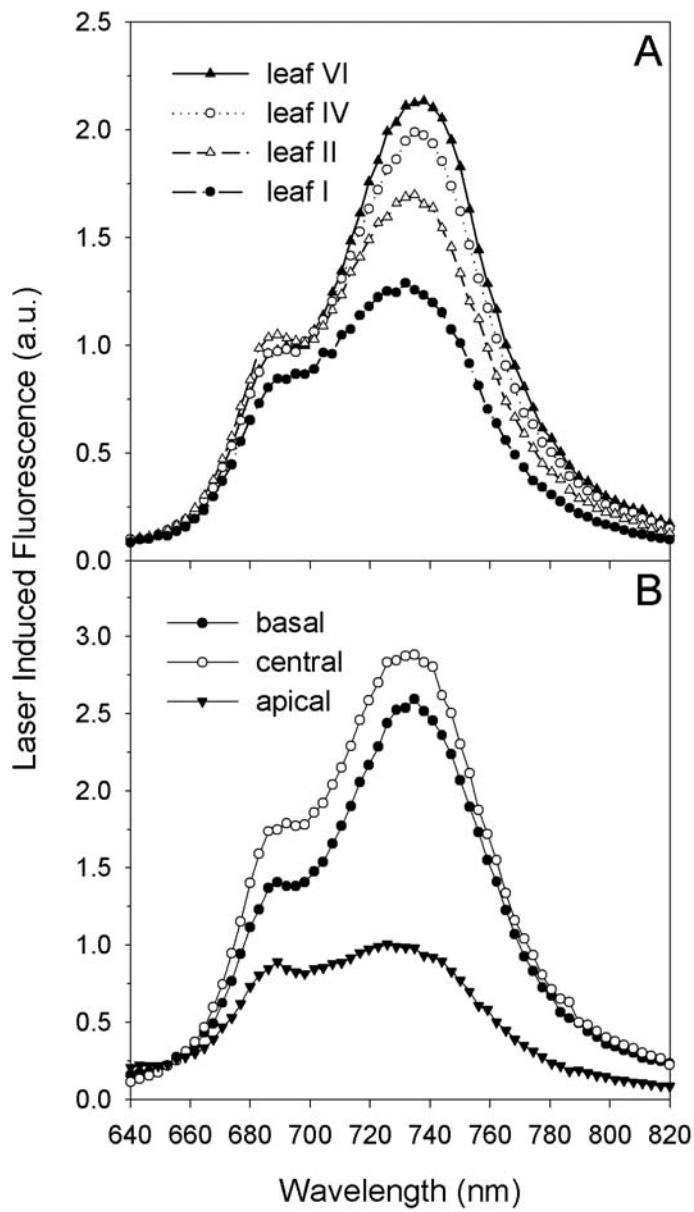
Figure 7. Laser induced fluorescence spectra of single corn leaves excited at 532 nm. (A) leaves at different position into the plant (I to VI from top of the plant). (B) Different part from the same leaf (leaf II from the top).
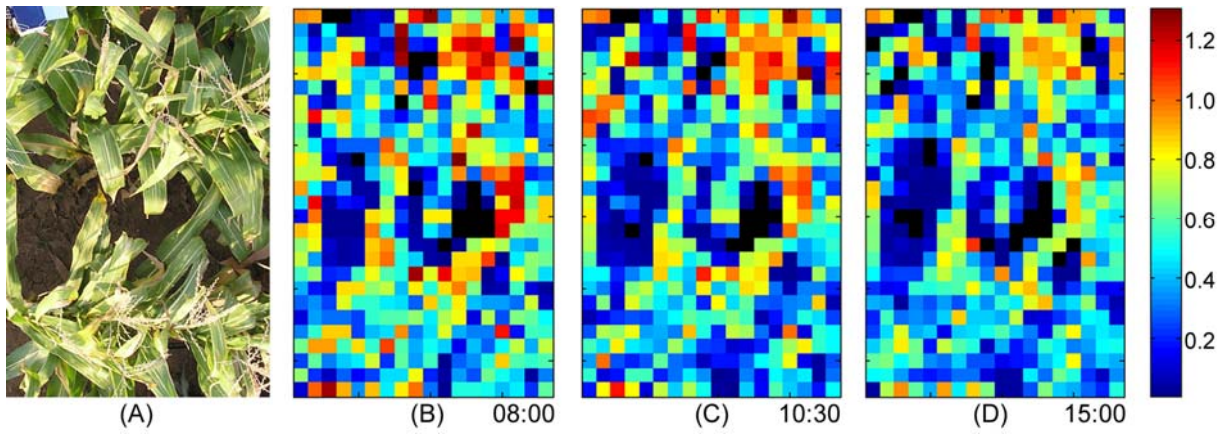
1042

1043

1044 Figure 8. (A) Corn canopy area (about 1 m^2) scanned by the FLIDAR imaging system, within

1045 small angles from nadir; note the presence of a fluorescence standard (blue) and a reflectance

1046 standard (white) at the left-top corner. (B-D) Canopy fluorescence maps at the 760 nm band,

1047 with excitation at 532 nm, acquired in sequence at 8:00, 10:30 and 15:00 (UTC), respectively,

1048 on 12 September, 2007. Each map, made up of 18 x 27 pixels, required an acquisition time of

1049 20 min. Fluorescence intensities in the colour bar are expressed as arbitrary units.

1050
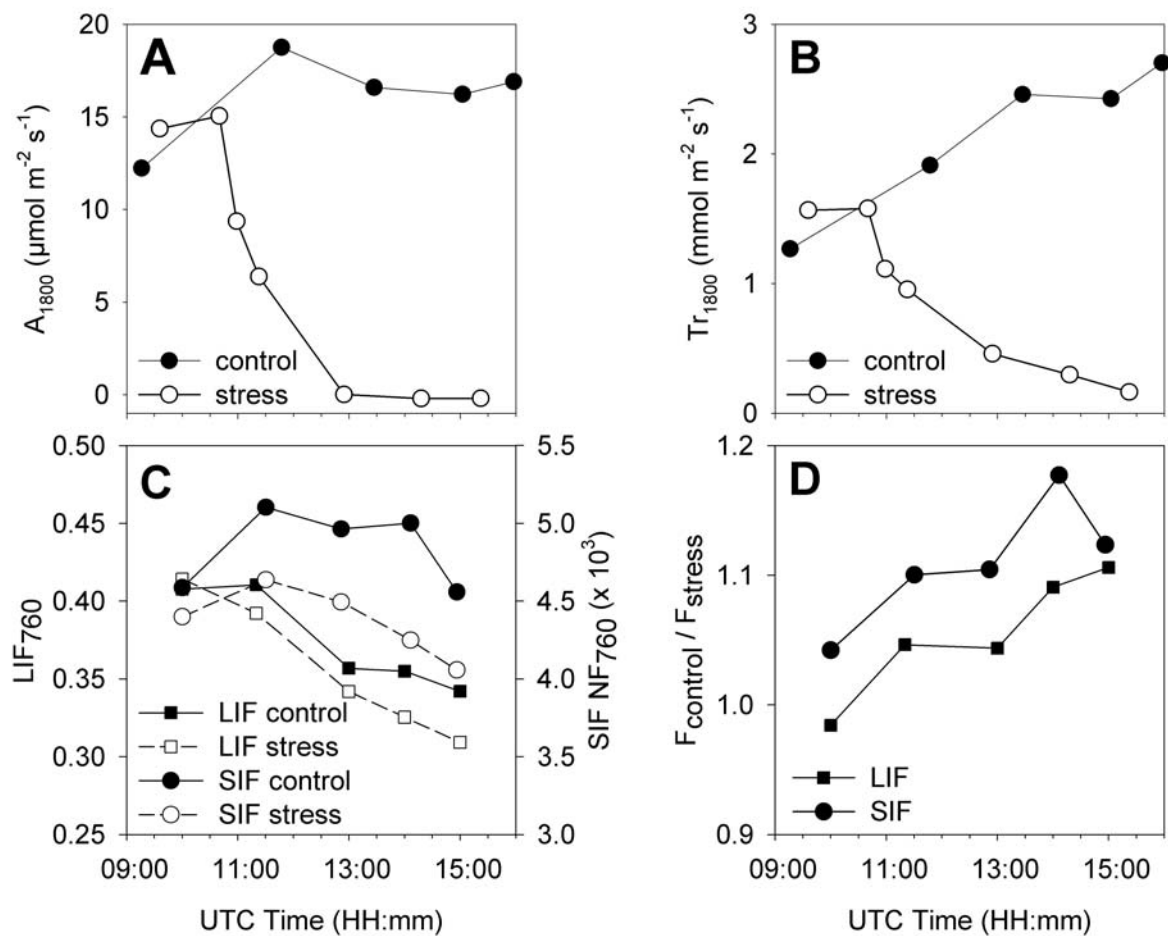
1051
1052

Figure 9: Time evolution of photosynthetic CO_2 uptake rate (A), leaf transpiration (B), SIF and LIF signals at 760 nm (C) and ratio of the fluorescence signals (D) from control and stressed corn plants. Desiccation stress was applied at 10am by cutting the plants but keeping them under the same conditions in the canopy. Photosynthetic uptake rates and transpiration were measured at the leaf level, while SIF and LIF were measured on the canopy level (about 1×1 meter). LIF and SIF data were normalized to a fluorescence standard signal and to the incident solar radiance, respectively

1060
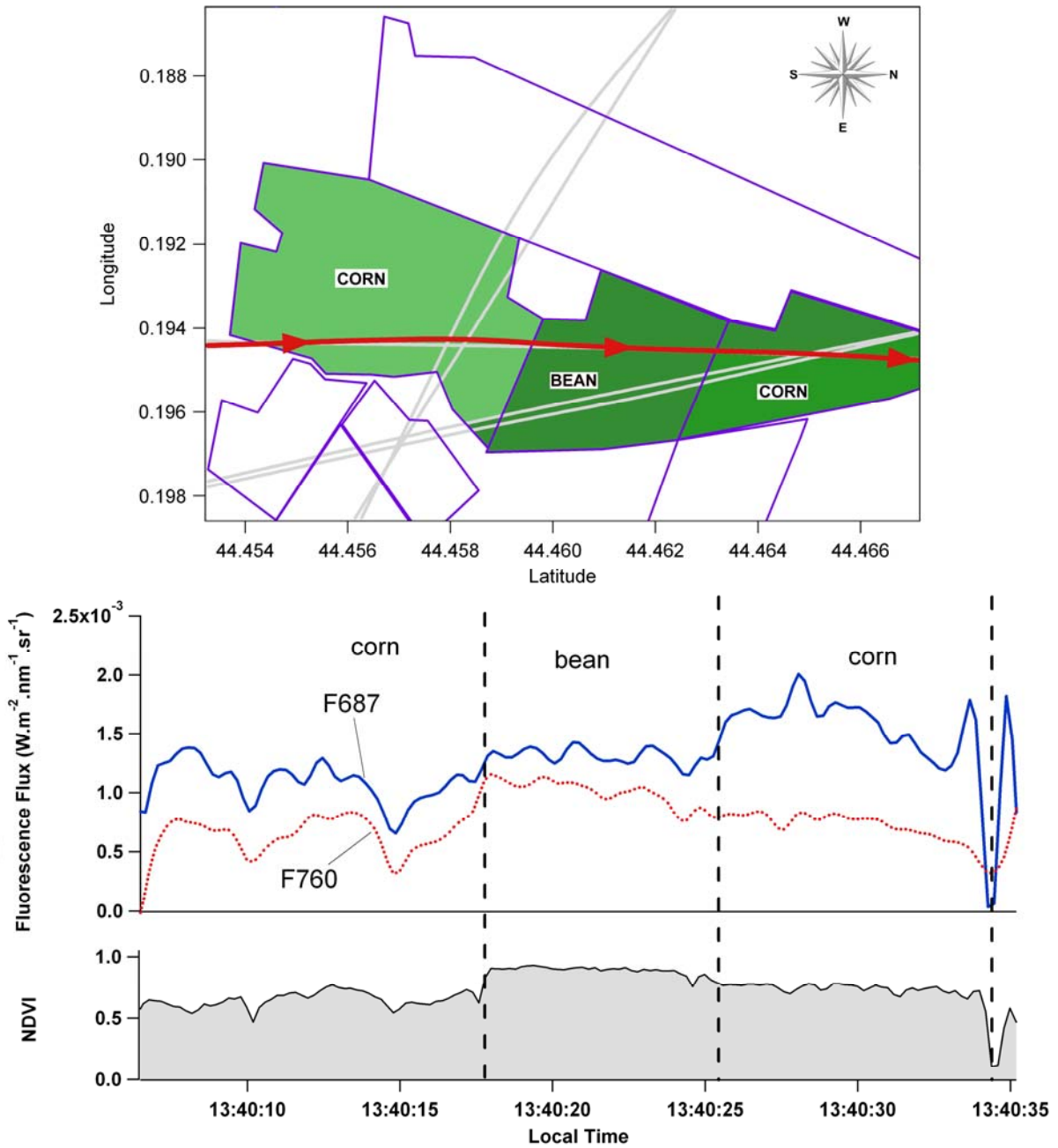
Figure 10. Top: AirFLEX transects over the Marmande test fields on 15 September, 2007. Bottom: Fluorescence flux at 687 nm, fluorescence flux at 760 nm and NDVI measured during the transect marked in red.
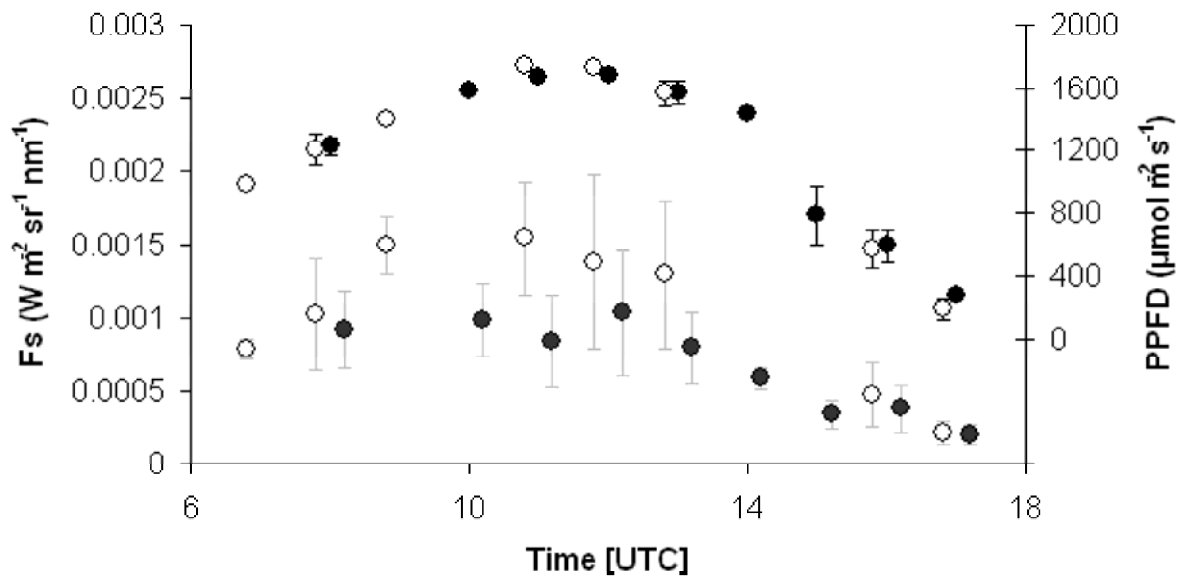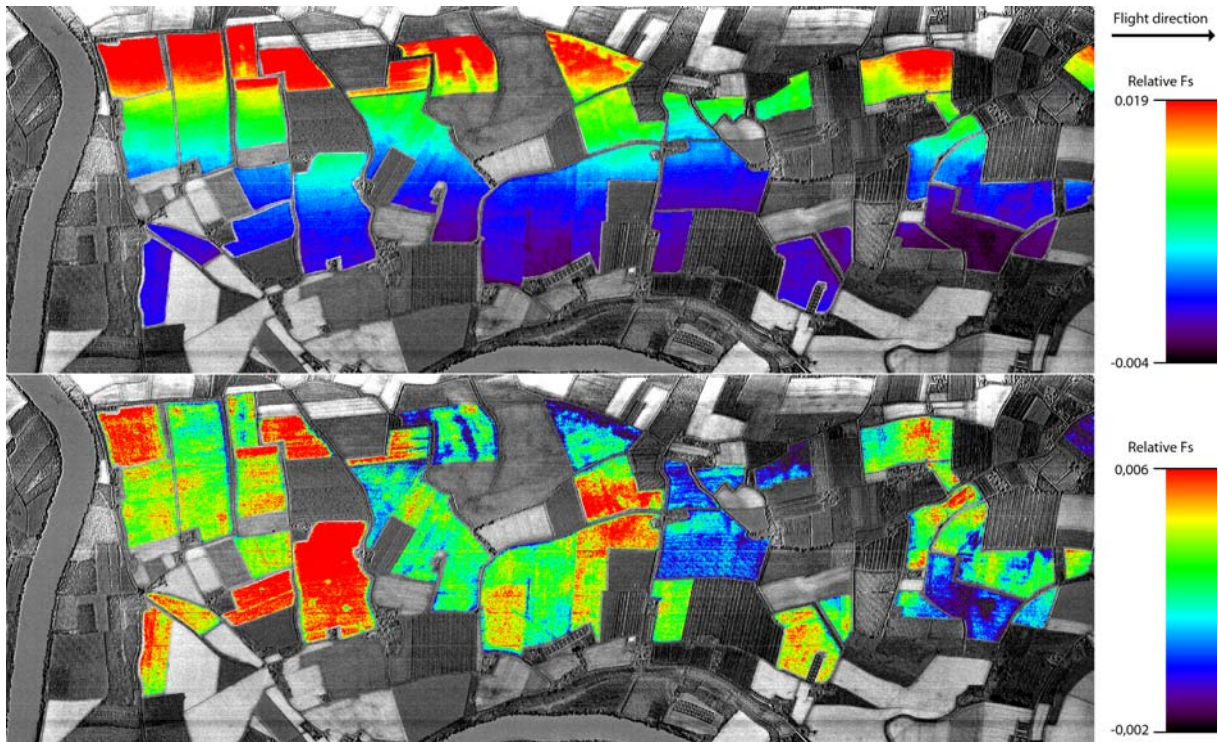
Figure 11. Fs (left axis) and PPFD (right axis) averages at different hours of the day over 118 pine fields (black circles) and over 47 wheat fields (white circles) during five days of flights from 18 to 23 April, 2007.

1073
1074
1075 Figure 12 Relative distribution of Fs signal as derived from HYPER imaging spectroscopy
1076 data (30 June 2007) without correction of anisotropic cross-track effects (top) and with
1077 empirical correction of the effects (bottom). Results show Fs values for all corn fields in the
1078 Marmande area and have been filtered with a 3x3 pixel mean filter to reduce statistical noise.